Nucleic Acids Research, 2024, **52**, 6945–6963
https://doi.org/10.1093/nar/gkae426
Advance access publication date: 23 May 2024
Gene regulation, Chromatin and Epigenetics

The p21CIP1-CDK4-DREAM axis is a master regulator of genotoxic stress-induced cellular senescence

Ariane Schmidt[1,†], Sebastian Allmann[1,†], Christian Schwarzenbach[1], Petra Snyder[2], Jia-Xuan Chen[3], Georg Nagel[1], Anna Schöneis[1], Birgit Rasenberger[1], Petra Beli[3], Alexander Loewer[2], Thomas G. Hofmann[1], Maja T. Tomicic[1] and Markus Christmann[1,*]

[1]Department of Toxicology, University Medical Center of the Johannes Gutenberg University of Mainz, Obere Zahlbacher Str. 67, D-55131 Mainz, Germany
[2]Department of Biology, Technical University Darmstadt, Schnittspahnstrasse 13, 64287 Darmstadt, Germany
[3]Institute of Molecular Biology, Ackermannweg 4, 55128 Mainz, Germany

[*]To whom correspondence should be addressed. Tel: +49 6131 179066; Email: mchristm@uni-mainz.de
[†]The first two authors should be regarded as Joint First Authors.

Abstract

Cellular senescence, a major driver of aging, can be stimulated by DNA damage, and is counteracted by the DNA repair machinery. Here we show that in $p16^{INK4a}$-deficient cells, senescence induction by the environmental genotoxin B[a]P or ionizing radiation (IR) completely depends on $p21^{CIP1}$. Immunoprecipitation-based mass spectrometry interactomics data revealed that during senescence induction and maintenance, $p21^{CIP1}$ specifically inhibits CDK4 and thereby activates the DREAM complex. Genome-wide transcriptomics revealed striking similarities in the response induced by B[a]P and IR. Among the top 100 repressed genes 78 were identical between B[a]P and IR and 76 were DREAM targets. The DREAM complex transcriptionally silences the main proliferation-associated transcription factors E2F1, FOXM1 and B-Myb as well as multiple DNA repair factors. Knockdown of $p21^{CIP1}$, E2F4 or E2F5 diminished both, repression of these factors and senescence. The transcriptional profiles evoked by B[a]P and IR largely overlapped with the profile induced by pharmacological CDK4 inhibition, further illustrating the role of CDK4 inhibition in genotoxic stress-induced senescence. Moreover, data obtained by live-cell time-lapse microscopy suggest the inhibition of CDK4 by $p21^{CIP1}$ is especially important for arresting cells which slip through mitosis. Overall, we identified the $p21^{CIP1}$/CDK4/DREAM axis as a master regulator of genotoxic stress-induced senescence.

Graphical abstract

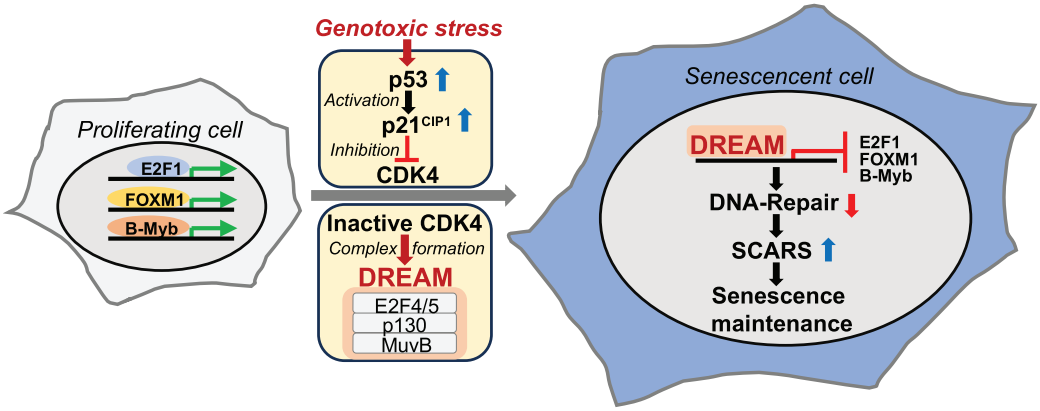

Introduction

Initially, senescence was described as a permanent cell cycle arrest, responsible for limiting the life span of cultured human cells (1). In contrast to a transient cell cycle arrest (quiescence), senescence does not influence metabolic competence of the cells, and is not reversible in response to proliferative conditions (for review, see (2–5)). Beyond telomere-driven replicative senescence, cellular senescence is also induced by hyper-proliferative signals (oncogenic senescence) and genomic damage (DNA damage-induced senescence). A hallmark of cellular senescence is the activation of the DNA damage response (DDR) and the subsequent induction of an irreversible cell cycle arrest which is mediated *via* inhibition of Cyclin dependent kinases (CDKs) by specific inhibitory proteins (cyclin-dependent kinase inhibitors, CDKNs) (6). In this context, the most important CDKNs are

Received: November 9, 2023. **Revised:** May 2, 2024. **Editorial Decision:** May 3, 2024. **Accepted:** May 14, 2024

CDKN1a/p21^{CIP1} and CDKN2a/p16^{INK4a} which may play different roles during cellular senescence. Hence, senescence can be divided into two phases, initiation of senescence and its maintenance (7). The initial phase is activated by induction of p21^{CIP1} and the subsequent cell cycle arrest. However, in some cases, the p21^{CIP1} expression declines at later stages of senescence (6,8,9). In contrast, p16^{INK4A} levels gradually increase during this period (10) and the cell cycle arrest becomes irreversible (11,12), mainly via accumulation of p16^{INK4A} (8,13,14). Generally, p21^{CIP1} inhibits cyclin-CDK1 and cyclin-CDK2, whereas p16^{INK4A} inhibits cyclin-CDK4/6, which in both cases leads to inactivation of the p105(RB)-E2F1 complex and activation of p107(RBL1)-E2F4 and p130(RBL2)-E2F4/5, thereby arresting cell cycle progression (15,16). However, it is still under debate whether senescence indeed can be separated into these two phases (time sequences) and whether both, p21^{CIP1} and p16^{INK4A} are indispensable for senescence. This is of particular importance since *CDKN2a*/p16^{INK4A}, but not *CDKN1a*/p21^{CIP1} is frequently altered in cancer. Thus, according to the 'My Cancer Genome' database (https://www.mycancergenome.org, (17)), CDKN2A is altered in 11.23% of malignant solid tumour patients and in 10.52% of all cancer patients, whereas CDKN1A is altered only in 0.96% of malignant solid tumour patients and is not found significantly altered in cancer patients overall.

The DREAM complex is an evolutionary highly conserved transcriptional repressor complex associated with p21^{CIP1} (18). The core DREAM complex is formed by the MuvB complex which consists of the MuvB-related proteins LIN9, LIN37, LIN52, LIN54, and RBBP4 (19). Throughout the cell cycle several proteins can bind to the MuvB core to increase or decrease transcriptional activity. In the late G1 and S-phase B-Myb (*MYBL2*) binds to the MuvB complex *via* LIN9 and LIN52 forming the proliferative B-Myb-MuvB complex (MMB) (20–22). Upon progression into the late S/G2-phase, FOXM1 gets associated with the MMB complex forming the FOXM1-MMB complex. These binding events facilitate phosphorylation and subsequent degradation of B-Myb, resulting in transcriptional activity of the remaining proliferative FOXM1-MuvB complex in the G2 and M-phase (20,23). In the absence of growth signals, the DREAM complex is assembled. To this end, the protein kinase DYRK1A phosphorylates LIN52 at serine 28 allowing it to bind to p130, with a higher affinity than to B-Myb (24). p130 in its hypophosphorylated form interacts with E2F4 as well as DP1. Although the DREAM complex, *via* its LIN54 subunit, binds to the same promotor elements as the aforementioned complexes (25), it now leads to transcriptional repression of its target genes. The DREAM complex disassembly is mediated *via* phosphorylation of p130 on up to 20 different phosphorylation sites (26). This phosphorylation is performed by CDK4/6 during the transition from the G0/G1 to the S-phase (21,27,28). On one hand, the DREAM complex is important for arresting cells in the G0-phase, and on the other, it controls p53-mediated gene repression. In this case, p53 does not bind directly to the promotor regions, but leads *via* p21^{CIP1} induction to activation of the DREAM complex (29–33). Although, the DREAM complex has been shown to regulate Ras-induced senescence (24), the role of the DREAM complex in the regulation of cellular senescence upon genotoxic stress remains unclear.

Whereas the mechanisms leading to replicative and oncogene-induced senescence are well established, the pathways underlying DNA damage-induced senescence still remain to be defined. A major obstacle in our understanding of DNA damage-induced senescence is the broad variety of DNA lesions that induce cellular senescence starting from different phases of the cell cycle. To this end, we compared the pathways leading to cellular senescence upon exposure to the chemical genotoxin benzo(a)pyrene (B[a]P) and the physical genotoxin ionizing radiation (IR), both inducing a different spectrum of DNA damage. B[a]P is formed during industrial production processes, vehicle exhaust emissions, food preparation and tobacco smoking and therefore represents the most important environmental genotoxin formed by incomplete combustion. In humans exposed to B[a]P, a significantly increased risk of different types of cancer have been found, and in 2014 B[a]P was classified as 'carcinogenic to humans" by the Environmental Protection Agency (EPA) and listed as a Group 1 carcinogen by the IARC (34). To unleash its carcinogenic activity, B[a]P must be metabolized into benzo(a)pyrene 7,8-diol-9,10-epoxide (BPDE), which represents the ultimate carcinogenic metabolite (35–38). BPDE binds *via* its epoxide group to the exocyclic N^2 position of guanine (39,40), forming a bulky adduct in the DNA. Opposite to B[a]P, IR induces predominantly oxidative DNA damage due to radiolysis of water. Moreover, IR can induce, directly and subsequently to the oxidative damage, single-strand breaks (SSBs) and double-strand breaks (DSBs). B[a]P/BPDE-induced bulky adducts can be repaired by nucleotide excision repair or bypassed by translesion synthesis, whereas IR-induced oxidative damage, SSBs and DSBs are repaired by base excision repair, SSB repair and DSB repair, respectively (41).

Our results indicate that, although inducing different types of DNA damage, the IR and B[a]P-triggered responses both converge at the level of sustained p21^{CIP1} activation, which is sufficient to abrogate proliferation and to induce and maintain the senescence response. Mechanistically, p21^{CIP1} inhibits CDK1, CDK2 and CDK4 activities during the induction phase of senescence, manifesting a proliferation arrest in the G2/M-phase, most likely due to post-translational modifications. Interestingly, this G2/M-arrest is not stable and the majority of the cells slip through G2/M into the subsequent G1-phase. At this time point, during the maintenance phase, p21^{CIP1} inhibits predominantly CDK4 leading to formation of the DREAM complex. The DREAM complex now silences the transcription and thereby the protein expression of E2F1, of the proliferative MuvB interactors FOXM1 and B-Myb and all of their targets involved in cell cycle control and DNA repair, thereby irreversibly arresting the cells in the first G2/M-phase and the second G1/S-phase. Collectively, our findings suggest a central role for the DREAM complex in blocking cell proliferation to facilitate DNA damage-induced senescence.

Materials and methods

Cell culture, drug treatment, siRNA-mediated knockdown and pharmacological inhibition

MCF7 breast cancer cells were obtained from CLS Cell Lines Service GmbH, Eppelheim, Germany and RPE-1 cells were obtained by ATCC. The human diploid VH10tert foreskin fibroblast cell line was kindly provided by Prof. Mullenders (Department of Toxicogenetics, Leiden University Medical Centre, the Netherlands). MCF7 FUCCI-H2B reporter cells were kindly provided by Bob van de Water (Division of

Drug Discovery & Safety, Leiden Academic Centre for Drug Research, Leiden University, the Netherlands). They express mClover-Geminin(1-110) and mKO2-Cdt1(30–120) from a bicistronic lentiviral vector as well as H2B-iRFP670 as a nuclear marker (42). MCF7 cells were cultivated in Dulbecco's minimal essential medium (DMEM)-F12 containing 5% fetal bovine serum (FBS) under normal atmosphere (5% CO_2) at 37°C. VH10tert and RPE-1 cells were cultivated in DMEM containing 10% FBS. Cells were regularly checked for mycoplasma contamination using the Venor GeM Classic kit from Minerva Biolabs.

B[a]P was purchased from Sigma (B1760) and activated r-7,t-8-Dihydroxy-t-9,10-epoxy-7,8,9,10-tetrahydrobenzo(a)pyrene (BPDE; CAS no. 58917-67-2) was synthesized from trans-7,8-dihydroxy-7,8-dihydrobenzo(a)pyrene (43) by Dr Seidel (BIU Biochemical Institute for Environmental Carcinogens, Grimmer-Stiftung, Grosshansdorf, Germany), as described (44). IR was performed within a Gammacell irradiator 2000 (Cs-137 source, Molsgaard Medical, Denmark). If not otherwise stated, B[a]P, BPDE and Palbociclib remained in the medium throughout the whole experiment.

For gene silencing, predesigned siRNAs specific for $p16^{INK4A}$ (sc-37622, Santa Cruz Biotechnology), $p21^{CIP1}$ (sc-29427, Santa Cruz Biotechnology), E2F4 (sc-29300, Santa Cruz Biotechnology) and E2F5 (sc-35250, Santa Cruz Biotechnology) were used; control human non-silencing siRNA (Silencer Select Predesigned siRNA Negative Control #1 siRNA; Ambion) was used as negative control. The transfections of siRNAs were performed using Lipofectamine RNAiMAX Reagent (Invitrogen). The CDK4/6 inhibitor Palbociclib (S4482, Selleckchem) was used at 1 μM, and the microtubule de-polymerising agent nocodazole (M1404, Sigma) was used at 0.2 μM.

Determination of clonogenic survival, cell cycle progression and senescence

For quantifying drug-induced clonogenic survival, the colony-forming assay was performed. Thus, 2000 cells were seeded in 6-cm dishes and exposed to genotoxic stress or the CDK4/6 inhibitor. 2–3 weeks later, the formed colonies were counted and adjusted in relation to the untreated control, which was set to 100%. For reseeding experiments cells were either non-exposed, exposed with B[a]P or exposed with Palbociclib for 120 h. Thereafter 2000 cells were reseeded in fresh medium and cultivated for 2–3 weeks. The formed colonies were counted and adjusted in relation to the untreated control, which was set to 100%. For analyzing cell cycle distribution, cells were stained with propidium iodide (PI) and the DNA content was determined by flow cytometry using BD FACSCanto™ II. Senescence was measured microscopically by β-Gal staining as described before (45). Experiments were repeated at least three times, mean values ± SD are shown.

Preparation of RNA and real-time qPCR

Total RNA was isolated using the NucleoSpin® RNA Kit (Macherey-Nagel, Düren, Germany). For real-time qPCR, 1 μg of total RNA was transcribed into cDNA (Verso cDNA Kit, Thermo Scientific, Dreieich, Germany). qPCR was performed in technical triplicates using the GoTaq® qPCR Master Mix Protocol (Promega, Madison, USA) and the CFX96 Real-Time PCR Detection System (Biorad, München, Germany). The specific primers are listed in Supplementary Table S1. Non-template controls were included in each run, expression was normalized to *gapdh* and *β-actin*; the untreated control was set to one. Analysis was performed using CFX Manager™ Software; SD shows intra-experimental variation.

RNA-seq

For analyzing the response to B[a]P and IR, NGS library prep was performed with Illumina's TruSeq stranded mRNA LT Sample Prep Kit following TruSeqStrandedmRNAReferenceGuide (Oct.2017) (Document # 1000000040498v00). Libraries were prepared with a starting amount of 1000 ng and amplified in 10 PCR cycles. Libraries were profiled in a High Sensitivity DNA on a 2100 Bioanalyzer (Agilent technologies) and quantified using the Qubit dsDNA HS Assay Kit, in a Qubit 2.0 Fluorometer (Life technologies). All 12 samples were pooled in equimolar ratio and sequenced on NextSeq 500 Highoutput FC, PE for 2 × 150 cycles plus 7 cycles for the index read.

For analyzing the response to Palbociclib, NGS library prep was performed with Illumina's Stranded mRNA Prep Ligation Kit following Stranded mRNA Prep Ligation ReferenceGuide (June 2020) (Document # 1000000124518 v00). Libraries were prepared with a starting amount of 1000 ng and amplified in 9 PCR cycles. Libraries were profiled in a HighSensitivity DNA chip on a 2100 Bioanalyzer (Agilent technologies) and quantified using the Qubit dsDNA HS Assay Kit, in a Qubit 2.0 Fluorometer (Life technologies). All 9 samples were pooled in equimolar ratio and sequenced on a NextSeq500 Highoutput FC, SR for 1 × 79 cycles plus 10 cycles for the index read and 2 dark cycles upfront Read 1.

Raw data are available at GEO (Gene expression omnibus) under GSE234862 (Impact of benzoapyrene and ionizing radiation on gene expression of MCF7 cells) and GSE235350 (Impact of Palbociclib (PD-0332991; CDK4/6 inhibitor) on gene expression of MCF7 cells).

Gene sets used for evaluation of NGS data

The following gene sets were obtained from the Molecular Signatures Database (MSigDB database v7.5.1) (46): FISCHER_DREAM_TARGETS (DREAM-F), FISCHER_DIRECT_P53_TARGETS_META_ANALYSIS, FISCHER_G1_S_CELL_CYCLE, FISCHER_G2_M_CELL_CYCLE (47); SHEPARD_BMYB_TARGETS (48). FOXM1 and E2F-RB target genes were directly obtained from Fischer et al., 2016 (47). A second set of DREAM targets (DREAM-E) was directly obtained from Engeland et al., 2018 (49). A set of DREAM-dependent p53-targets (DREAM-U) and a set of DREAM-independent p53 target genes were directly obtained from Uxa *et al.* (33). Venn diagrams were drawn using the program from (http://bioinformatics.psb.ugent.be/webtools/Venn).

Preparation of protein extracts, western blot analysis and co-immunoprecipitation

Whole-cell and nuclear extracts were prepared as described (50). For detection of phospho-specific antibodies, cells were directly lysed in 1x SDS-PAGE sample buffer and subsequently sonified. Mouse mAb and rabbit pAb were diluted 1:500–1:2000 in 5% BSA, 0.1% Tween-TBS and incubated overnight at 4°C; the specific antibodies are listed in Supplementary Table S2. Protein-antibody complexes were detected by

Pierce® ECL Western Blotting Substrate (Thermo Fisher). The size of the detected proteins was verified by molecular weight markers (Spectra™ Multicolor Broad Range Protein Ladder, Thermo Fischer #26634) and listed in Supplementary Table S2. Co-Immunoprecipitation was performed using the Catch and Release® v2.0 Kit (Merck, Darmstadt, Germany) according to the manufacturer's protocol.

p21^{CIP1}-Interactomics

For identification of p21^{CIP1} binding partners, cells were either non-treated or treated with 1 μM B[a]P for 48 and 120 h. Thereafter p21^{CIP1} was immunoprecipitated and protein in-gel digestion, dimethyl labelling and liquid chromatography tandem mass spectrometry were performed. For details, see Supplemental methods. Data are deposited at the Protein Identification Database (PRISE). Project name: Protein–protein interactions of p21^{CIP1} in MCF7 cells during cellular senescence, Project accession: PXD042908.

Immunofluorescence (IF) staining

For IF staining, cells were grown on coverslips and fixed at different time points after exposure to genotoxic stress or the CDK4/6 inhibitor Palbociclib in ice-cold methanol:aceton (7:3) at 4°C for 7 min. After washing in PBS, the cover slips were blocked with 5% BSA in PBS with 0.3% Triton X-100 for 1 h. Thereafter, 200 μl of antibody solution (1:100–1:400 in PBS with 0.3% Triton X-100) was added and the cover slips were incubated overnight at 4°C. After 3 times washing with PBS, 200 μl of the chromofluor-labelled secondary antibody solution (1:1000 in PBS with 0.3% Triton X-100) was added and incubated at room temperature in the dark for 2 h. After three final washing steps in PBS, the cover slips were mounted with Vectashield mounting medium containig TO-PRO-3, as described (51). Microscopical analyses were performed using the Zeis 710 LSM.

Live-cell time-lapse microscopy

MCF7 cells express fusions of a N-terminal fragment of Geminin (GMNN) with the fluorescent protein mClover and a N-terminal fragment of CDT1 with the fluorescent protein mKO2. This allows to identify cells in G1-phase by low GMNN and high CDT1 levels, while GMNN levels are high and CDT levels low in S- and G2-phase. During mitosis, both markers are absent.

0.8×10^5 cells were seeded in 3.5 cm ibiTreat polymer-bottom plates (ibidi, Martinsried, Germany) 2 days before experiments. At the day of the experiment, medium was replaced by FluoroBrite medium (Thermo Fisher Scientific, Darmstadt, Germany) lacking phenol red and riboflavin supplemeted with 5% FBS. Cells were treated with 1 μM B[a]P or irradiated with 5 Gy X-rays (250 KeV). We imaged cells on a Nikon Ti inverted fluorescence microscope (Nikon, Düsseldorf, Germany) with a Nikon DS-Qi2 camera and a 20× Plan Apo objective (numerical aperture 0.75) using appropriate filter sets. The microscope was enclosed with an incubation chamber maintaining temperature (37°C), atmosphere (5% CO_2) and humidity. Cells were imaged every 15 min for the duration of the experiment using Nikon Elements software (Nikon, Düsseldorf, Germany).

Cells were tracked throughout the duration of the experiment using custom-written MATLAB (MathWorks) scripts, as previously described (52). In brief, we applied flat field correction and background subtraction to raw images before segmenting individual nuclei from nuclear marker images using thresholding and seeded watershed algorithms. Segmented cells were then assigned to corresponding cells in following images using a greedy match algorithm. Only cells tracked from the first to last time point were considered. Upon division, we followed the daughter cell closest to the last position of the mother and merged tracks from mothers and offspring. For visualization, the minimum was substracted from individual mClover-GMNN and mKO2-CDT1 trajectories before normalization to the maximum.

Quantification and statistical analysis

The data were evaluated using Student's *t*-test and were expressed as a mean ± SD. $^*P \leq 0.05$ was considered statistically significant, $^{**}P \leq 0.01$ very significant and $^{***}P \leq 0.001$ highly significant. Statistical analyses were performed using GraphPad Prism version 6.01 for Windows, GraphPad Software, La Jolla California USA (www.graphpad.com).

Results

DNA-damage-induced senescence depends on p21^{CIP1}

To elucidate the molecular mechanisms underlying DNA damage-induced senescence, we used metabolically competent MCF7 cells that are able to metabolize B[a]P into BPDE. In parallel experiments, we also studied the IR-induced senescence response to obtain more general insight into the mechanisms of DNA damage-induced senescence. In initial experiments we identified treatment conditions leading to comparable induction of senescence and cell death between exposure to B[a]P and IR. 120 h after exposure to 1 μM B[a]P or 5 Gy IR, cells largely remained viable and only about 10–15% cells underwent cell death (sub-G1-fraction, Figure 1A and B, left panel). Both, B[a]P and IR arrested the cells predominantly in the G1-phase (Figure 1A and B, left panel). Up to 75% cells expressed the senescence marker SA (senescence associated)-β-Galactosidase upon B[a]P or IR treatment (Figure 1A/B, middle panel, Supplementary Figure S1A). Colony formation assay showed a complete abrogation of clonal growth starting at concentrations of 0.1 μM B[a]P or IR doses ≥5 Gy (Figure 1A and B, right panel). Cellular senescence was accompanied by persisting DNA-SCARS (DNA segments with chromatin alterations reinforcing senescence), presumably representing unrepaired DNA DSBs (53). Upon B[a]P and IR similar, low (3,4) numbers of SCARS (identified as 53BP1/γH2AX containing foci) were observed (Figure 1C and D, Supplementary Figure S1B).

Based on these findings, we decided to use 1 μM B[a]P or 5 Gy IR for further experiments. Notably using these conditions, sustained induction of *CDKN1a*/p21^{CIP1} was observed on RNA and protein level (Figure 1E and F). In contrast, neither *CDKN2a*/p16^{INK4A} nor *CDKN2a*/p14^{ARF} were expressed on protein level (Supplementary Figure S2A). This is in line with data showing that the *CDKN2a* gene is homozygously deleted in the MCF7 breast cancer cell line (54), which could be verified by genomic PCR (Supplementary Figure S2B). In the absence of p16^{INK4A}, induction of p21^{CIP1} was a prerequisite for DNA damage-induced cellular senescence, since knockdown of p21^{CIP1} reduced the frequency of senescent cells from 60 to 10% (Figure 2A and B).

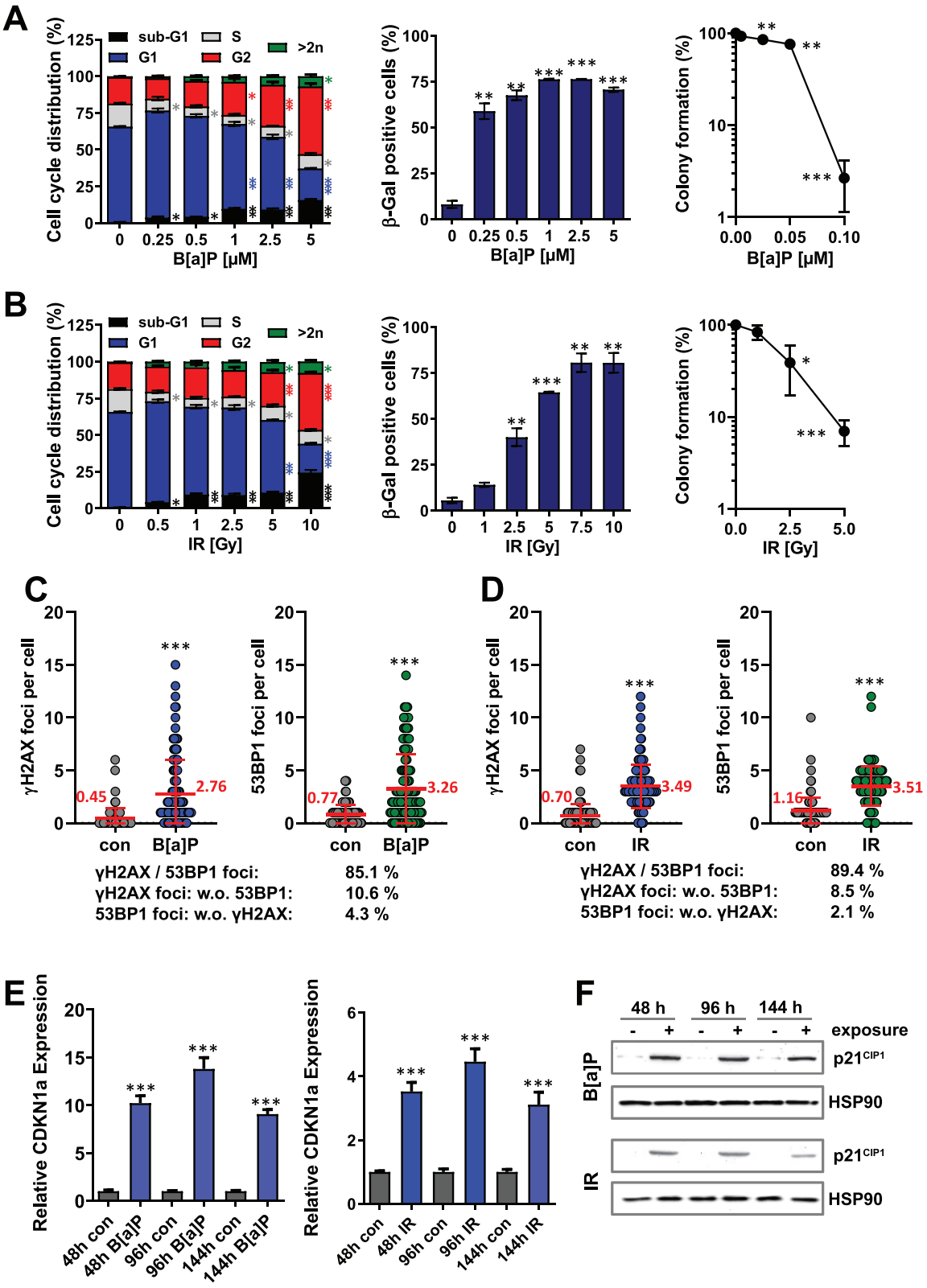

Figure 1. (A, B) MCF7 cells were exposed to different concentrations of B[a]P (**A**) or different doses of IR **(B)** for 120 h (left and middle panel) or for 2 weeks (right panel). Experiments were performed in triplicates. Cell death and cell cycle distribution were measured by flow cytometry using PI staining (left graph). Frequency of senescent cells was detected microscopically by SA-β-Gal staining (middle panel). Proliferation and clonogenic survival were measured by colony formation assay (right panel). (**C, D**) MCF7 cells were exposed to 1 µM B[a]P (C) or 5 Gy IR (D) for 120 h. Formation of γH2AX and 53BP1 foci was measured by confocal laser scanning microscopy (LSM). Foci were counted in 200 cells. Numbers of foci/cell and co-localization events are shown. (**E, F**) Expression of *CDNK1a* upon B[a]P or IR exposure was measured by qPCR (E) or immunoblotting (F). For qPCR, *ACTB* and *GAPDH,* and for immunodetection, HSP90 were used as internal loading control. Experiments were performed in triplicates. (A–E) Differences between treatment and control were statistically analysed using Student's *t* test (non labelled = non significant, $*P < 0.1$ $**P < 0.01$, $***P < 0.001$).

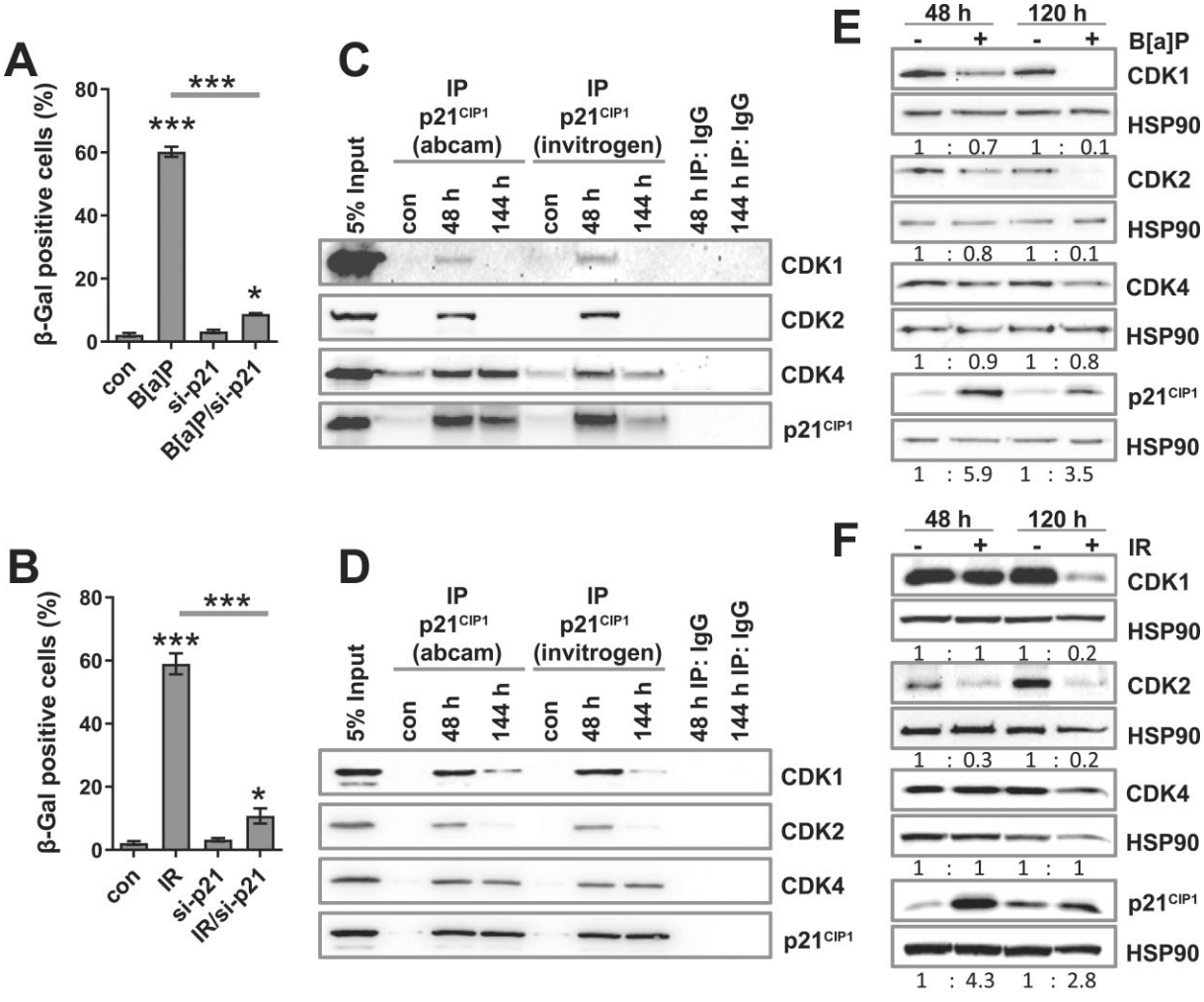

G

Protein	con	24 h	120 h	24h/con	120h/con
p21CIP1	5.28	8.77	4.66	3.92	2.36
CDK1	1.48	1.38	-	1.99	-2.73
CDK2	4.42	1.29	3.81	1.35	-0.01
CDK4	1.88	2.18	4.71	2.19	1.53
CCNA2	3.74	0.39	-	2.19	-3.577
CCNE1	-	3.36	-	1.78	1.67
CCND1	1.17	2.31	1.13	2.60	1.40
CCND3	3.76	3.84	2.82	2.08	1.39
PCNA	-	1.77	1.50	2.53	-

Figure 2. (**A, B**) p21CIP1 was silenced using siRNA and MCF7 cells were exposed to B[a]P or IR. Frequency of senescent cells was detected microscopically by β-Gal staining. Experiments were performed in triplicates. Differences between treatment and control, as well as between treatment and treatment + siRNA were statistically analysed using Student's *t* test (non labelled = non significant, $*P < 0.1$ $**P < 0.01$, $***P < 0.001$). (**C, D**) MCF7 cells were exposed to 1 μM B[a]P (C) or 5 Gy IR (D) and binding of p21CIP1 to CDK1, CDK2 and CDK4 was identified by Co-IP. (**E, F**) MCF7 cells were exposed to 1 μM B[a]P (E) or 5 Gy IR (F) and the expression of p21CIP1, CDK1, CDK2 and CDK4 was immunodetected. HSP90 was used as internal loading control, quantification of band intensities from two blots is shown. (**G**) MCF7 cells were exposed to 1 μM B[a]P and p21CIP1 binding partners were identified using interactomics. Interaction with cell cycle associated factors is shown in the left panel (Expression (log2_Ratio) above input control is shown).

p21^{CIP1} forms complexes with CDK1, CDK2 and CDK4 during DNA damage-induced senescence

Based upon our data, p21^{CIP1} represents a critical cyclin-dependent kinase inhibitor in response to genotoxic stress. Co-immunoprecipitation experiments using different p21^{CIP1} antibodies (for specificity, see Supplementary Figure S2C) clearly showed that p21^{CIP1} interacted with CDK1, CDK2 and CDK4 48 h after B[a]P and IR exposure (Figure 2C/D). However, at later time points, during senescence maintenance (144 h), p21^{CIP1} only interacted with CDK4, which already showed the strongest interaction with p21^{CIP1} during senescence induction (48 h). This is consistent with the finding that CDK1 and CDK2 are not expressed anymore 120 h after B[a]P and IR exposure (Figure 2E/F). These data indicate that inhibition of CDK1/2 might be important for the induction of the initial cell cycle arrest, whereas inhibition of CDK4 is responsible for induction of the senescence phenotype and its maintenance. To investigate whether p21^{CIP1} interacts with factors besides CDKs during DNA damage-induced senescence, we performed mass spectrometry-based interactomics experiments in untreated cells, and cells exposed for 24 and 120 h with B[a]P. Whereas an increased interaction with CDK1 (1.99), CDK2 (1.35) and CDK4 (2.19) was observed 24 h after B[a]P exposure, after 120 h, an enrichment was only observed for CDK4 (1.53), whereas the amount of CDK1 (-2.73) and CDK2 (-0.01) was reduced (Figure 2G). In line with this, 120 h after exposure, p21^{CIP1} also interacted with the well-characterized CDK4 interactors cyclin D1/*CCND1*, cyclin D3/*CCND3* and PCNA, but neither with cyclin A2/*CCNA2*, which interacted with p21^{CIP1} in untreated cells and after 24 h, nor with cyclin E1/*CCNE1*, which was found as interaction partner only 24 h upon exposure (Figure 2G). Of note, binding of p21^{CIP1} to CDK6 was not observed in interactomics experiments. Interactomics also revealed additional putative p21^{CIP1} interactors (Supplementary Figure S3 and Supplementary Tables S3 and S4). In detail, significantly regulated pathways were identified by the ConsensusPathDB-human platform (http://cpdb.molgen.mpg.de/). Top significantly over-represented pathways, identified using the KEGG database, were 'cyclins and cell cycle regulation', 'p53 signaling pathway', 'rb tumor suppressor/checkpoint signaling in response to DNA damage' and 'cell cycle: G1/S checkpoint'. These pathways were identified only upon B[a]P exposure but not in non-treated cells. Top significantly over-represented pathways identified using the BioCarta database were 'splicosome', 'protein processing in endoplasmic reticulum', 'p53 signaling pathway' and 'cell cycle'. Among those, in non-treated cells only 'splicosome' was detected. Top significantly over-represented pathways identified using the Reactome database were associated with RNA metabolism and mRNA splicing and detected in non-exposed and exposed cells. Since mRNA splicing occurs in nuclear speckles, we analysed the intracellular localization of p21^{CIP1} upon B[a]P exposure. Indeed, 120 h after exposure, accumulation of p21^{CIP1} in distinct nuclear foci was observed (Supplementary Figure S4A) and co-localization experiments revealed that p21^{CIP1} localized to nuclear speckles and paraspeckles, but not to Cajal bodies, PML bodies and nucleoli (Supplementary Figure S4B). This localization supports the results obtained by the interactomics analysis, indicating a tight trapping of a subfraction of p21^{CIP1} in these compartments. However, since the interactomics data showed no difference between non-exposed and exposed cells for most of the potential interactors (Supplementary Table S4), it is to suppose that the retention of p21^{CIP1} to these compartments represents a DNA damage-unrelated event. Interestingly, all proteins that were increased 48 h after B[a]P exposure >log 1.5 versus the control were cell cycle associated factors (CCNE1, CCND3, CDK4 and CCND1). 120 h after B[a]P exposure, among these factors, only CDK4 was still significantly enriched. In addition, other factors were enriched at this time point (SEC24B, SEC24C, NME1. KHSRP, TIAL1, MAPK1IP1L, DHX9 and ANXA11). The potential interaction with those factors and biological relevance has to be verified in the future.

B[a]P and IR-induced DNA damage activate the DREAM response

Inhibition of CDK4/6 leads to inactivation of the p105-E2F1 complex and activation of p130-E2F4/5, which causes cell cycle arrest (15,16). Moreover, this can lead to the activation of the DREAM complex if p130 binds the transcriptional repressor E2F4 or E2F5 and arrests cells in the G0-phase (55). In this cell cycle phase, the active p130–E2F4 complex can silence genes *via* recruitment of histone deacetylases (56) or the recruitment of the CtBP corepressor complex (57).

To analyse putative DNA damage-induced activation of the DREAM complex, we determined the expression of the DREAM components E2F4, E2F5, p130, as well as phosphorylation of p130. Previously, we showed that E2F1 protein expression was abrogated upon exposure to B[a]P (58), due to proteasomal degradation. In addition, a time-dependent decrease in *E2F1* mRNA upon B[a]P and IR exposure was observed (Figure 3A/B). In contrast to *E2F1*, which represents a prototypic DREAM target, the expression of *E2F4* was only marginally reduced and *E2F5* expression was not altered upon B[a]P and IR exposure (Figure 3A/B). Also on protein level, the expression of E2F4 and E2F5 was only marginally reduced upon B[a]P treatment and not altered upon IR exposure (Figure 3C and D). Most importantly, the phosphorylated, inactive form of p130 was strongly reduced, whereas unphosphorylated, active p130 levels remained unchanged. Concerning RB, both the phosphorylated and the unphosphorylated forms were virtually undetectable upon treatment with B[a]P or IR. Overall the findings indicate that both, B[a]P and IR, activate the DREAM complex. This is also supported by strongly decreased transcriptional expression of cyclin genes (*CCNA1, CCNA2, CCNB1* and *CCNB2)* (Figure 3A and B). In contrast, *CCND1* and *CCND2* showed an enhanced expression, representing a well-known marker of replicative senescence (59).

Genome-wide transcriptomic analysis revealed overlapping DREAM responses upon B[a]P and IR-induced senescence

To analyse the transcriptional alterations during cellular senescence induced by B[a]P and IR in more detail, transcriptomic analysis was performed 120 h after treatment (for principal component analysis and clustering of the top 40 regulated genes, see Supplementary Figure S5). At first glance, different pathways were activated or repressed upon B[a]P and IR. Pathway analysis using the REACTOME database via the WEB-based GEne SeT AnaLysis Toolkit (http://www.webgestalt.org/) indicated that B[a]P induced predominantly components involved in histone methylation, whereas IR activated an interferon response (Supplementary Figure S6).

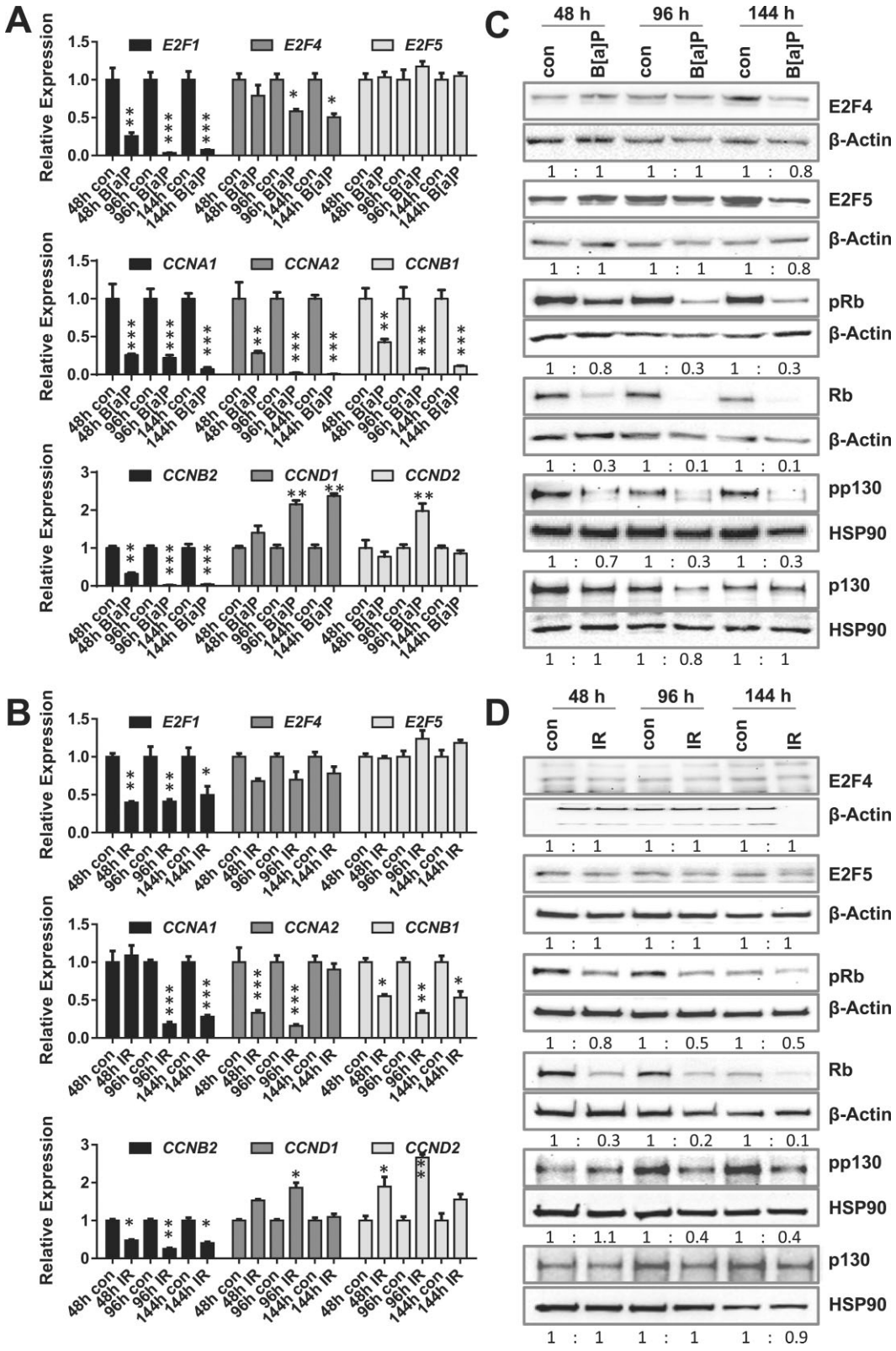

Figure 3. MCF7 cells were exposed to 1 μM B[a]P (**A, C**) or 5 Gy IR (**B, D**). Expression of *E2F1, E2F4, E2F5, CCNA1, CCNA2, CCNB1, CCNB2, CCND1* and *CCND2* was analysed by qPCR (A, B). *ACTB* and *GAPDH* were used as internal loading control, differences between treatment and control were statistically analysed using Student's t test (non labelled = non significant, $*P < 0.1$ $**P < 0.01$, $***P < 0.001$). Expression of *E2F4, pRB, RB, pp130* and *p130* was analysed by immunodetection (C, D). β-Actin or HSP90 were used as internal loading control, quantification of band intensities from two blots is shown.

Concerning the repressed pathways, B[a]P and IR showed a similar response. Thus, pathways involved in Rho signalling and cell cycle control were repressed. Furthermore, pathway analysis using the KEGG database indicated that B[a]P and IR strongly repressed cell cycle control and, in addition, DNA repair. Concerning the induced pathways, B[a]P triggered mainly metabolism of xenobiotics by cytochrome P450 and chemical carcinogenesis, whereas IR triggered predominantly cytokine, chemokine and interleukin pathways (Supplementary Figure S7).

Overall, analysing genes with BH adjusted *P*-values <0.001 and $\log_2$ fold change >2, 327 genes were up-regulated by B[a]P and 539 genes were up-regulated by IR (Figure 4A). Among these genes 147 were commonly up-regulated by B[a]P and IR. However, besides these high number of genes, no significantly regulated pathways were identified by the REACTOME pathway analysis (https://reactome.org/PathwayBrowser/). Notably, cell cycle, DNA repair and DNA replication were not influenced (Figure 4B). A different picture was observed concerning the down-regulated genes upon B[a]P and IR (Figure 4A). Among these genes 240 were down-regulated by both DNA damage inducers. REACTOME pathway analysis showed striking results and the top 3 repressed pathways were cell cycle, DNA repair and DNA replication (Figure 4B). Concerning DNA repair, the strongest repression was observed for DNA double-strand break repair (Supplementary Figure S8A), which is in line with our previous observations (58).

The high similarity of the responses was also observed in the most significantly regulated genes. Among the 20 most significantly regulated genes, 7 were identical (Supplementary Figure S8B) and among the top 100 significantly down-regulated genes, 78 were the same (Figure 4C, Supplementary Figure S9). Among the top 100 significantly up-regulated genes only 29 were identical and 6 of them are direct p53 targets like *TP53INP1* and *CDKN1a* (Figure 4D and E). Importantly, 76 out of the 78 commonly down-regulated genes were DREAM targets (Figure 4D and E). Since many of these genes were also targets activated by the MuvB interactors FOXM1 and B-Myb (Figure 4F and Supplementary Figure S10A and B), a disruption of these complexes was very likely. Interestingly, the FOXM1/DREAM targets were mostly G2/M-specific genes, whereas the E2F-RB/DREAM targets were mostly G1/S-specific (Supplementary Figure S10C). These results strongly correlate with previous findings (60).

Importantly, *FOXM1* and *MYBL2* themselves were among the top 100 repressed genes. Indeed, qPCR experiments verified the repression of all selected DREAM targets (*ASPM, AURKB, CENPA, CENPF, MYBL2, FOXM1, PLK1, TK1*), and for FOXM1 and B-Myb the repression was also verified at protein level (Supplementary Figure S11A-C). These data demonstrate that $p21^{CIP1}$-dependent CDK4/6 inhibition activated the DREAM complex, and strongly reduced the expression of all proliferation-related factors like E2F1, FOXM1 and MYBL2 and thereby completely inactivated the MuvB complex. In addition, HMGB1, HMGB2 and LMNB1 were among the DREAM targets and showed a strongly reduced expression upon B[a]P and IR exposure both on mRNA and protein level, which represents a known feature of senescence (Supplementary Figure S12A–D). Collectively, our genome-wide transcriptional profiling suggests activation of the DREAM complex and concomitant repression of DREAM target genes as common denominator of the DNA damage-induced senescence response.

Silencing of E2F4, E2F5 or $p21^{CIP1}$ reduces DREAM-mediated gene repression and senescence

Based on the transcriptomics results, activation of the DREAM complex alone might be sufficient to mediate DNA damage-induced senescence. To test this hypothesis, we silenced E2F4, E2F5 and as a positive control $p21^{CIP1}$, using RNAi and analysed the impact on B[a]P and IR-induced repression of DREAM targets and senescence. Silencing of E2F4 reduced the frequency of senescent cells upon B[a]P exposure from 65 to 45% and upon IR exposure from 50 to 35%. Silencing of E2F5 reduced the frequency of senescent cells upon B[a]P exposure from 65 to 35% and upon IR from 50 to 37%. Finally, combined silencing of E2F4 and E2F5 reduced the frequency of senescent cells from 65 to 25% upon B[a]P exposure and from 50 to 20% upon IR exposure (Figure 5A/B). Combined silencing of E2F4 and E2F5 also reduced repression of multiple DREAM target genes (Figure 5C). Similar to E2F4/E2F5 silencing, also silencing of $p21^{CIP1}$ diminished repression of these genes (Supplementary Figure S13).

To challenge the importance of the $p21^{CIP1}$/CDK4/DREAM axis in DNA damage-induced senescence, we used two additional cellular model systems, non-transformed human telomerase-transfected foreskin fibroblasts (VH10tert) and non-transformed human telomerase-transfected retinal epithelial cells (RPE-1). Both cell lines are not metabolically competent and are thus unresponsive to B[a]P. Therefore, the active metabolite BPDE was used.

VH10tert cells are $p16^{INK4A}$ deficient due to epigenetic silencing of *p16*^{INK4A} (Supplementary Figure S2A/B). Exposure of VH10tert cells to BPDE (0.5 μM) arrested the cells predominantly in G1 and effectively induced cellular senescence (Supplementary Figure S14A). Moreover, activation of the DREAM pathway was shown by dephosphorylation of RB and p130, and an increased expression of $p21^{CIP}$ (Supplementary Figure S14B). Silencing of either $p21^{CIP1}$ or E2F4/5 reduced the frequency of senescent cells from 70% to 10% ($p21^{CIP1}$ siRNA) or 25% (E2F4/E2F5 siRNA) (Supplementary Figure S14C–E) and, as consequence, diminished the repression of the DREAM targets (Supplementary Figure S14F).

Opposite to MCF7 and VH10tert cells, RPE-1 cells are $p16^{INK4A}$ proficient (Supplementary Figure S2A and B). Also in this cell line, exposure to BPDE (0.5 μM) arrested the cells predominantly in G1 and effectively induced cellular senescence (Supplementary Figure S15A). Similar to VH10tert cells, activation of the DREAM pathway was shown by dephosphorylation of RB and p130, and an increased expression of $p21^{CIP}$ (Supplementary Figure S15B) as well as repression of the DREAM target genes (Supplementary Figure S15C). In contrast to $p21^{CIP}$, the expression of $p16^{INK4A}$ was not altered (Supplementary Figure S15B). Whereas silencing of either $p21^{CIP1}$ or E2F4/5 reduced the frequency of senescent cells from 70% to 10% ($p21^{CIP1}$ siRNA) or 20% (E2F4/E2F5 siRNA); silencing of $p16^{INK4A}$ had no impact (Supplementary Figure S15D/E).

To further support the importance of CDK4, we additionally performed co-immunoprecipitation experiments in VH10tert and RPE-1 cells. Similar to MCF7 cells, 120 h after

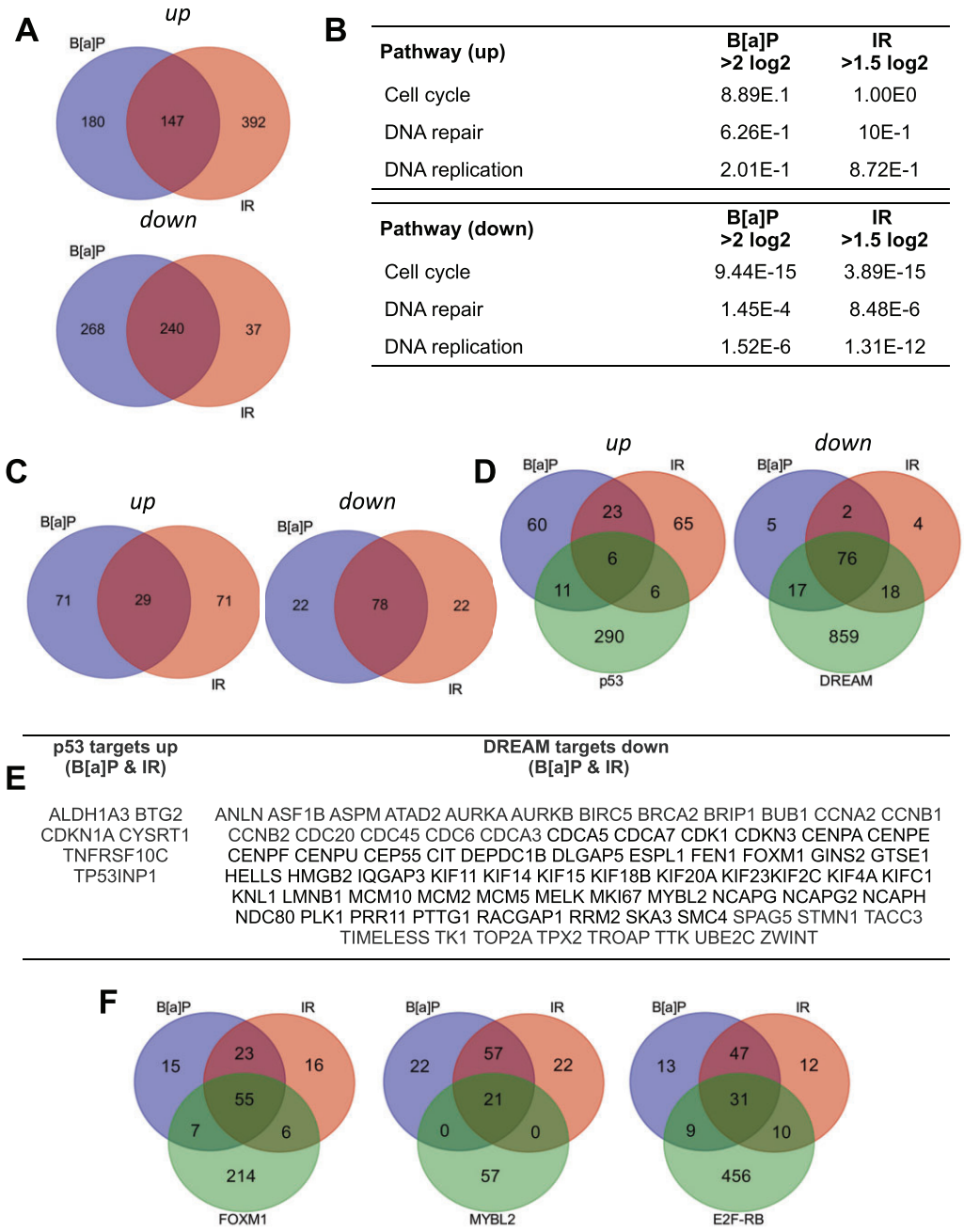

Pathway (up)	B[a]P >2 log2	IR >1.5 log2
Cell cycle	8.89E.1	1.00E0
DNA repair	6.26E-1	10E-1
DNA replication	2.01E-1	8.72E-1

Pathway (down)	B[a]P >2 log2	IR >1.5 log2
Cell cycle	9.44E-15	3.89E-15
DNA repair	1.45E-4	8.48E-6
DNA replication	1.52E-6	1.31E-12

Figure 4. MCF7 cells were exposed to 1 μM B[a]P or 5 Gy IR for 120 h. RNA was isolated and subjected to RNA-Seq. (**A**) Amount of genes commonly up-regulated (upper panel) or down-regulated (lower panel) upon B[a]P and IR exposure are displayed as Venn diagrams. (**B**) Significantly regulated pathways were identified by the Reactome pathway browser (https://reactome.org/PathwayBrowser/). (A, B) For B[a]P up and down-regulated genes with BH adjusted *P*-values <0.001 and $\log_2$ fold change > 2 are included, for IR up-regulated genes with BH adjusted *P*-values <0.001 and $\log_2$ fold change >2 are included, for IR down-regulated genes with BH adjusted *P*-values <0.001 and $\log_2$ fold change >1.5 are included. (**C**) Amount of genes commonly up- or down-regulated upon B[a]P and IR exposure are displayed as Venn diagrams. (**D**) Amount of genes commonly up- or down-regulated upon B[a]P and IR exposure and overlap with DREAM or p53 targets are displayed as Venn diagrams. (**E**) List of p53 targets up-regulated by B[a]P and IR, as well as DREAM targets down-regulated by B[a]P and IR. (**F**) Amount of genes commonly down-regulated upon B[a]P and IR exposure and overlap with FOXM1, MYBL2 and E2F1-RB targets are displayed as Venn diagrams. (C–F) Top 100 most significantly induced or repressed genes were included.

exposure, $p21^{CIP1}$ only interacted with CDK4, but not CDK1 and CDK2 (Supplementary Figure S16).

Pharmacological inhibition of CDK4 activates a DREAM response similar to DNA damage

Since our data unequivocally indicate that the $p21^{CIP1}$-mediated inhibition of CDK4 is important for activation of the DREAM complex and for the senescence response, we compared the transcriptional response observed in MCF7 cells upon B[a]P and IR with the response induced by CDK4 inhibition. To this end we used the CDK4/6 inhibitor Palbociclib. Palbociclib is well known to either induce quiescence or senescence depending on the cell type *in vitro* and *in vivo* (61). Incubation with 1 μM Palbociclib did not induce cell death, but massively arrested the cells in the

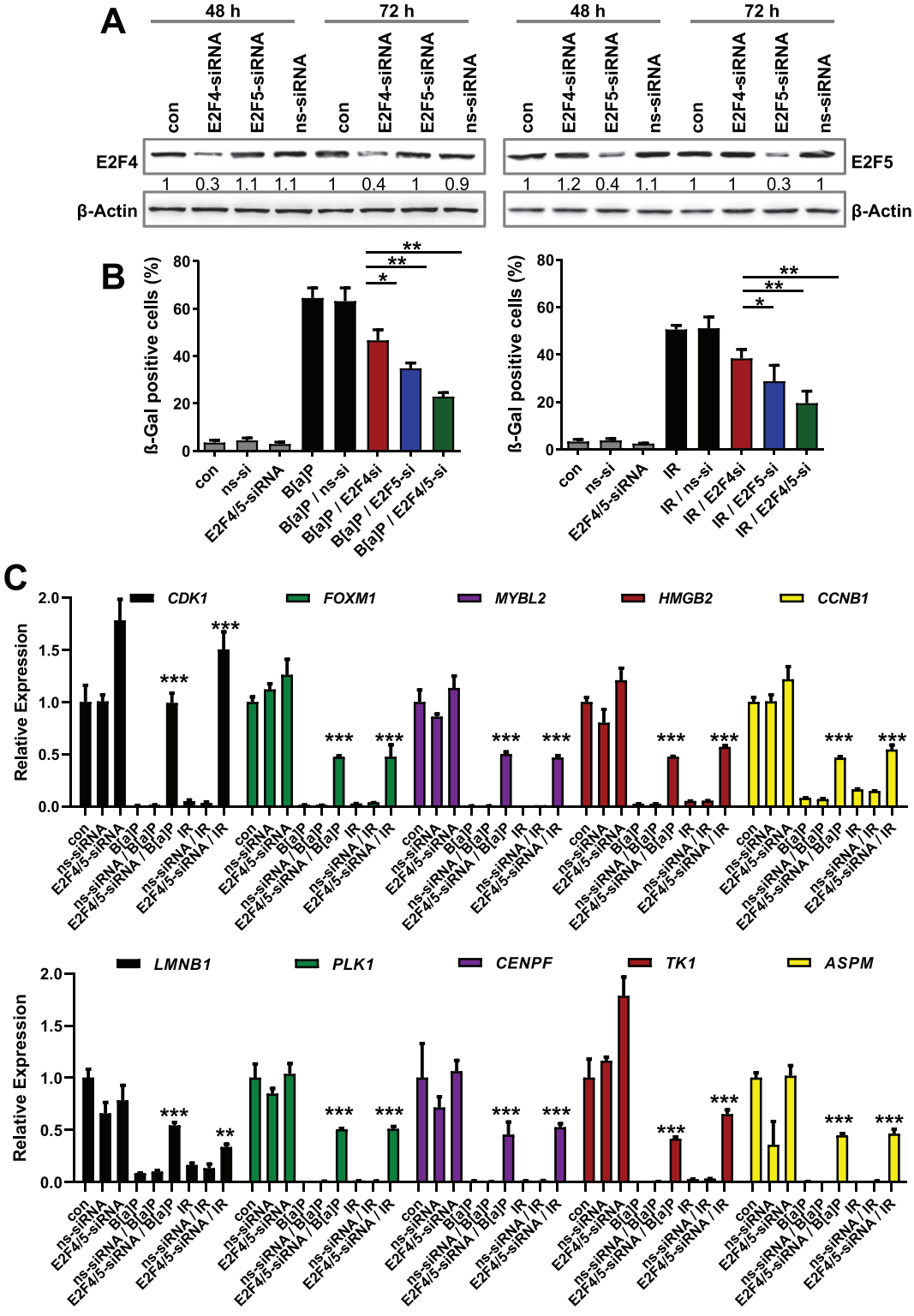

Figure 5. (**A**) Expression of E2F4 and E2F5 was detected 48 and 72 h after siRNA-mediated knockdown by immunodetection; β-Actin was used as internal loading control; quantification of band intensities indicates knock-down efficiency. (**B, C**) MCF7 cells were treated with E2F4-, E2F5- or non-specific siRNA for 24 h and thereafter exposed to B[a]P or IR for 120 h. (**B**) Senescence was measured microscopically by β-Gal staining. (**C**) Expression of *CDK1, FOXM1, MYBL2, HMGB2, CCNB1, LMNB1, PLK1, CENPF, TK1* and *ASPM* was measured by qPCR; *ACTB* and *GAPDH* were used as internal loading control. (B, C) Experiments were performed in triplicates, differences between treatment in absence or presence of siRNA were statistically analysed using Student's t test (non labelled = non significant, $*P < 0.1$ $**P < 0.01$, $***P < 0.001$).

G1-phase (Figure 6A, left panel) and in consequence completely abrogated clonogenic cell growth (Figure 6A, middle panel). Moreover, Palbociclib induced ∼80% SA-β-Gal positive cells (Figure 6A, right panel). Importantly, similar to B[a]P and IR, Palbociclib induced a strong repression of the DREAM targets *CDK1*, *FOXM1, MYBL2, HMGB2, CCNB1, LMNB1, PLK1, CENPF, ASPM* and *TK1* (Figure 6B). We should state that Palbociclib-induced cell cycle arrest and senescent phenotype in MCF7 cells were reversible after the removal of the inhibitor. This is shown by reseeding experiments (Supplementary Figure S17A). In these experiments, cells were either non-exposed, exposed to B[a]P or to Palbociclib. 120 h later, the cells were reseeded in fresh medium and cultivated for 2–3 weeks. Opposite to B[a]P, which showed colony formation below 1%, upon Palbociclib exposure, 98% of the cells were able to form colonies. The reversibility of the senescence phenotype after Palbociclib was already reported (62) and is associated with the fact that Palbociclib only marginally induce DNA damage and DDR activation, as measured by γH2AX and 53BP1 foci formation (Supplementary Figure S17B and C).

In an attempt to stratify the transcriptional alterations upon exposure to B[a]P, IR and Palbociclib in more detail, additional transcriptomic analyses were performed, showing strongly overlapping responses (Figure 6C). Similar to B[a]P and IR, no significantly up-regulated pathways were identified by the REACTOME pathway analysis upon Palbociclib, whereas cell cycle, DNA repair and DNA replication were strongly repressed (Figure 6D). Additional pathway analysis using the WEB-based Gene SeT AnaLysis Toolkit showed that Palbociclib weakly induced extracellular matrix organization and interferon signalling (using the REACTOME database) and estrogen signalling pathway (using the KEGG database) (Supplementary Figure S18). In contrast, a strong repression of cell cycle and DNA repair was revealed using both the REACTOME and KEGG database (Supplementary Figure S18). Concerning DNA repair, the DNA double-strand break repair, the Fanconi Anemia pathway as well as the mismatch repair pathway were significantly repressed (Supplementary Figure S18). Comparison of the top 200 repressed genes among B[a]P, IR and Palbociclib revealed that 98 were identical (Figure 6E). Most importantly, among those 98 genes 95 were DREAM targets (Figure 6E, Supplementary Figure S19A). Comparing all repressed genes showed that 159 DREAM targets were jointly repressed by B[a]P, IR and Palbociclib (Supplementary Figure S19B).

Cells slip from G2/M into G1 during B[a]P and IR induced senescence

Interestingly, apart from the high similarity of the responses in respect to the DREAM targets, also differences between B[a]P and IR at one hand and Palbociclib on the other became obvious by the transcriptomic data. These differences were likely caused by the stronger G1-arrest upon Palbociclib. Among all genes repressed at the same time by B[a]P, IR and Palbociclib, 34 were described as G1/S specific and 67 as G2/M specific (Supplementary Figure S19C and D). However, in comparison, a higher amount of G1/S specific genes and a lower amount of G2/M specific genes was observed in response to Palbociclib. In detail, upon B[a]P exposure, among the top 100 repressed genes 15 were annotated as G1/S-specific (such as *E2F1, FEN1, PCNA*) and 53 as G2/M-specific genes (such as *FOXM1, CDK1, PLK1, CCNA2, HMGB1*) (Supplementary Figure S20). Similar results were obtained for IR (13 G1/S-specific and 50 G2/M-specific). Corresponding to the strong G1-arrest induced by Palbociclib, 23 G1/S-specific genes and 27 G2/M-specific genes were repressed.

The finding that B[a]P and IR arrested cells predominantly in G1/S was unexpected since the DNA damage is supposed to activate the DDR during DNA replication and to mostly arrest cells in the G2/M-phase. Of note, an increase in G2/M-arrested cells was observed only at high concentrations (see Figure 1). Therefore, we assume that the DDR activation at moderate, senescence-inducing concentrations, is not sufficient to efficiently arrest the cells in G2/M and cells may slip through mitosis harbouring damaged DNA.

To test this hypothesis, we employed the fluorescent cell cycle indicator (FUCCI) system (63) (Figure 7A). It is based on expression of an N-terminal fragment of Geminin (GMNN) fused to the fluorescent protein mClover and an N-terminal fragment of CDT1 fused to the fluorescent protein mKO2. Due to cell cycle specific degradation of each reporter, cells in G1 will be characterized by low GMNN and high CDT1 levels, while GMNN levels are high and CDT levels are low in S and G2. During mitosis, both markers are absent. Using time-lapse microscopy, the FUCCI system allows to monitor cell cycle progression in individual living cells (Figure 7B). Upon exposure to B[a]P, cells initially continued to divide with similar rates as control cells (Figure 7C). After about 10 h, the rate of divisions diminished and from 24 h post-treatment on, almost no further divisions could be observed until the end of the observation period (72 h). Compared to B[a]P, IR prevented cells from entering mitosis early after damage induction. To gain further insights into cell cycle regulation upon B[a]P and IR treatment, we categorized cells in dividing and non-dividing cells and determined the corresponding cell cycle progression in each subgroup. Upon B[a]P treatment, 64% of cells divided at least once (Figure 7D and Supplementary Figure S21A). Most of these cells arrested in G1 after mitosis, with some progressing further to the S/G2-phase or even mitosis during the observation period of 72 h. Interestingly, about 10% of cells that divided showed mitotic bypass, i.e. they progressed from the S/G2-phase into a G1 – like state without mitosis. Mitotic bypass was even more frequent in cells that did not divide after B[a]P treatment (36% of cells), with almost 2/3 of cells showing this phenotype (Figure 7E and Supplementary Figure S21B). Upon IR, most cells divided within a period of 72 h (78%, Figure 7F and Supplementary Figure S21C). These cells mainly arrested in the following G1-phase, with only a fraction of about 30% progressing to the S/G2-phase or mitosis. Of the IR-treated cells that did not divide (22% of cells, Figure 7G and Supplementary Figure S21D), ∼1/3 remained arrested in G1 during the full observation period. The majority of cells in this subgroup moved into the G2-phase, although this often occurred only at later time points.

We have already shown that knockdown of $p21^{CIP1}$, E2F4 and E2F5 diminished transcriptional repression and SA-β-Gal staining. However, what about proliferation itself? To analyse this, we measured cellular proliferation in MCF7 cells (Supplementary Figure S21E). As expected, B[a]P and IR exposure blocked proliferation after 24 h and knockdown of $p21^{CIP1}$ diminished this arrest. Interestingly, upon knockdown of E2F4/E2F5 proliferation was still blocked after 24–48 h

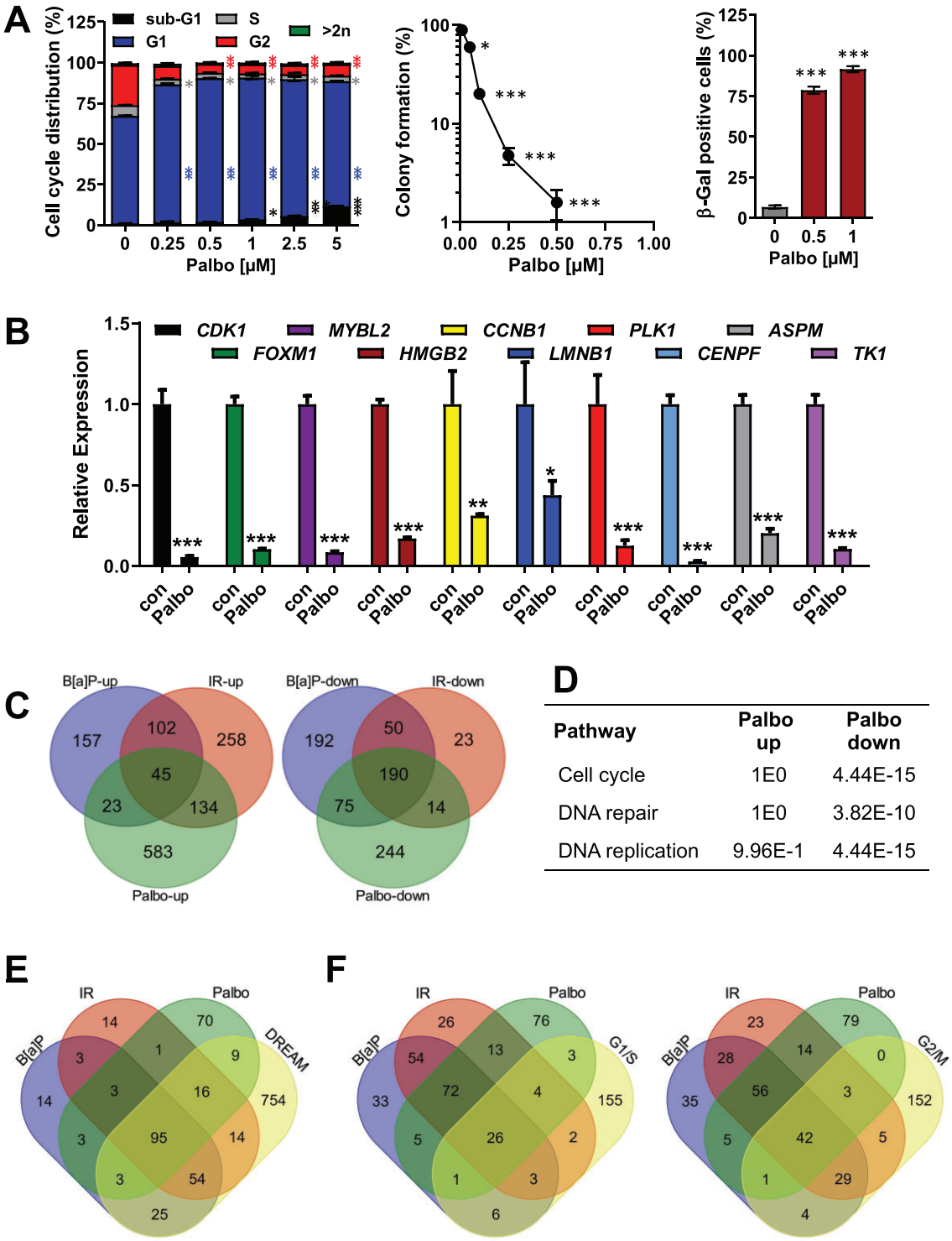

Figure 6. (A, B) MCF7 cells were treated with different concentrations of the CDK4/6 inhibitor Palbociclib for 120 h. (**A**) Cell death and cell cycle distribution were measured by flow cytometry using PI staining (left graph). Proliferation and clonogenic survival were measured by colony formation assay (middle panel). Frequency of senescent cells was detected microscopically by SA-β-Gal staining (right panel). (**B**) Expression of *CDK1, FOXM1, MYBL2, HMGB2, CCNB1, LMNB1, PLK1, CENPF, TK1* and *ASPM* were measured by qPCR; *ACTB* and *GAPDH* were used as internal loading control. (A, B) Experiments were performed in triplicates, differences between treatment and control were statistically analysed using Student's t test (non labelled = non significant, $*P < 0.1$ $**P < 0.01$, $***P < 0.001$). (C–F) MCF7 cells were exposed to 1 μM Palbociclib. RNA was isolated and subjected to RNA-Seq. (**C**) Amounts of genes commonly up- or down-regulated upon B[a]P, IR and Palbociclib exposure are displayed as Venn diagrams. (**D**) Pathways regulated by Palbociclib were identified by the Reactome pathway browser (https://reactome.org/PathwayBrowser/). (**E**) Amount of genes commonly down-regulated upon B[a]P, IR and Palbociclib and overlap with DREAM targets are displayed as Venn diagrams. (**F**) Amount of G1/S (left panel) and G2/M (right panel) specific genes commonly down-regulated upon B[a]P, IR and Palbociclib are displayed as Venn diagrams. (C–F) For B[a]P and Palbociclib, genes with BH adjusted *P*-values <0.001 and $\log_2$ fold change >2 are included, for IR down-regulated genes with BH adjusted *P*-values <0.001 and $\log_2$ fold change >1.5 are included. (E, F) Only the 200 most significantly down-regulated genes were included.

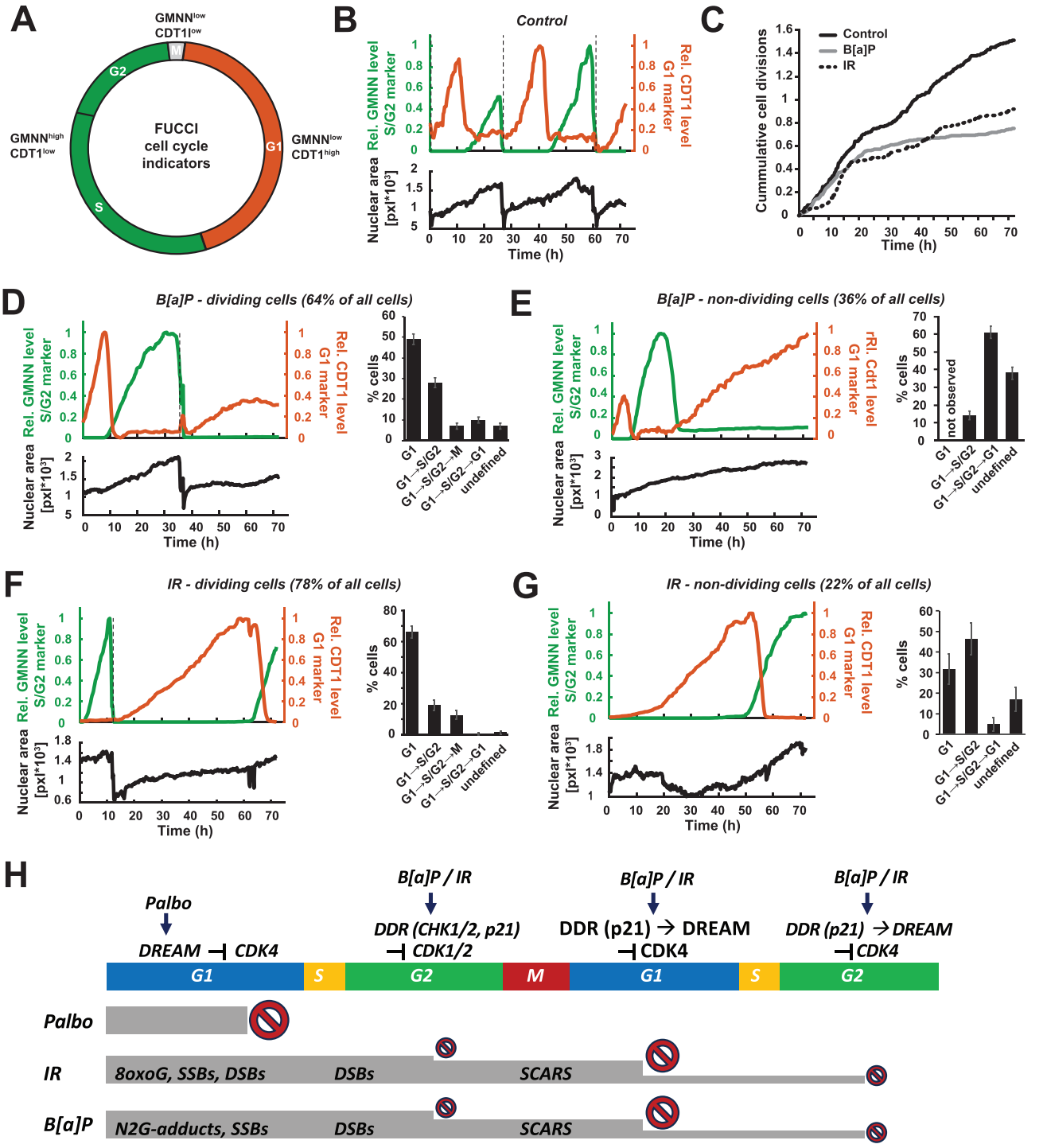

Figure 7. (**A**) Scheme of the fluorescent cell cycle indicator (FUCCI) system. (**B**) MCF7-FUCCI cells were imaged unperturbed for 72 h. As an example, normalized trajectories of mClover-GMNN (green) and mKO2-CDT1 (red) levels are shown for a selected cell. The size of the nuclear area is shown in the lower graph (black). Cell divisions are identified by sudden drops in nuclear area and indicated as vertical dashed lines in the upper graph. (**C**) Cumulative cell divisions of MCF7-FUCCI cells treated with 1 μM B[a]P, 5 Gy IR or left untreated (control) for a period of 72 h. (D, E) MCF7-FUCCI cells were treated with 1 μM B[a]P and imaged for 72 h. Cells were categorized into cells that divided (64% of all cells, (**D**) and those that did not divide (36% of all cells, (**E**). For each category, further cell cycle progressions were determined and their frequencies indicated as bar graphs. Cells showing both elevated GMNN and CDT1 levels were classified as undefined. Error bars indicate standard error of the proportion. Normalized trajectories of mClover-GMNN (green) and mKO2-CDT1 (red) levels are shown for selected cells representing the most common type of cell cycle progression for each subgroup. (F, G) MCF7-FUCCI cells were treated with 5 Gy IR and imaged for 72 h. Cells were categorized into cells that divided (78% of all cells, (**F**) and those that did not divide (22% of all cells, (**G**). Further cell cycle progression and exemplary trajectories are shown as above. (**H**) Model summarizing the role of $p21^{CIP1}$/DREAM in DNA damage-induced senescence.

but resumed at later time points. This might indicate that the initial cell cycle arrest, which is activated early after DNA damage is dependent on $p21^{CIP1}$ but not on the DREAM complex. Opposite, the DREAM complex is highly important for fixing the initial cell cycle arrest to become irreversible. Thus, addition of Palbociclib 48 h after DNA damage can override $p21^{CIP1}$-knockdown, and arrest the cells.

To support the importance of the DREAM complex for arresting cells slipping through mitosis, we additionally analysed the cellular proliferation of MCF7, VH10tert and RPE-1 cells upon B[a]P or BPDE exposure. All cell lines exhibited an increase in the cell number in a time frame up to 36 h, clearly showing that ∼50% of the cells can still progress through mitosis (Supplementary Figure S22A). Moreover, we utilized the spindle poison nocodazole. Nocodazole strongly arrested the cells in the G2/M phase. Importantly, a combined treatment with nocodazole and B[a]P or BPDE significantly reduced the amount of G1 cells compared to B[a]P or BPDE treatment alone, indicating that a large amount of the cells arrested in the G1 cells slipped through mitosis (Supplementary Figure S22B).

Overall, our data indicate that the p53-$p21^{CIP1}$-CDK4-DREAM axis is of central importance for converting the initial cell cycle arrest into an irreversible state, both in G2-arrested cells, and in cells slipping through mitosis.

Discussion

Our previous work has demonstrated that exposure to B[a]P or IR induces transcriptional repression of the MMR genes *EXO1, MSH2, MSH6* and of the central HR gene *RAD51*, leading to downregulation of the corresponding proteins and compromised DNA repair activity (58). Mechanistically, we showed that this downregulation is due to senescence-associated inactivation of E2F1 functions. Here we analysed the molecular mechanism underlying genotoxic stress-induced senescence, focusing on $p21^{CIP1}$ and the DREAM complex. Exposure of MCF7 cells to 1 μM B[a]P and 5 Gy IR efficiently induced senescence, but only marginal cell death. Senescence was accompanied by formation of SCARS. Thus, on average, 3–4 SCARS were observed 120 h after B[a]P and IR exposure. Remarkably, it has been postulated that already a single unresolved DSB can induce long-term induction of $p21^{CIP1}$ and senescence during replicative senescence (64).

In accordance with the SCARS, a sustained induction of $p21^{CIP1}$ was observed upon B[a]P and IR exposure, and knockdown of $p21^{CIP1}$ diminished senescence induction and increased toxicity. MCF7 cells are deficient for $p16^{INK4A}$, indicating that DNA damage-induced senescence does not require $p16^{INK4A}$. Our data show that contrasting previous reports analysing replicative senescence (6,8,9), during DNA damage-induced senescence, the $p21^{CIP1}$ expression did not decline during senescence maintenance. These data are also in line with those showing the $p21^{CIP1}$ and the $p16^{INK4A}$ pathways can be independently activated, and that also replicative senescence can be activated independently of $p16^{INK4A}$ (65).

To analyse the role of $p21^{CIP1}$ in DNA damage-induced senescence in more detail, we performed Co-IP experiments. $p21^{CIP1}$ interacted with CDK1, CDK2 and CDK4 48 h after B[a]P and IR exposure. At later time points (during senescence maintenance) $p21^{CIP1}$ exclusively interacted with CDK4, suggesting that inhibition of CDK1/2 might be involved in the initial cell cycle arrest, whereas CDK4 inhibition is important for maintenance of the cell cycle arrest and the senescence phenotype. Interestingly, inhibition of CDK4 is mainly associated with $p16^{INK4A}$ (15,16). Similar results were also obtained in $p16^{INK4A}$ deficient VH10tert cells in response to BPDE. Obviously, during DNA damage-induced senescence, $p21^{CIP1}$ can completely takeover the functions of $p16^{INK4A}$. This is also indicated by the results derived in $p16^{INK4A}$ proficient RPE-1 cells. Upon BPDE exposure, no alterations in the expression of $p16^{INK4A}$ were observed, and knockdown of $p21^{CIP1}$, but not of $p16^{INK4A}$ reduced the senescence frequency. Therefore, we conclude that $p16^{INK4A}$ is more important during normal aging and oncogene-induced senescence. Thus, the expression of $p16^{INK4A}$ is mainly controlled by PRC1/PRC2-mediated histone methylation, and during normal aging and oncogene-induced senescence, the expression of $p16^{INK4A}$ can be induced by demethylation (66). Opposite, during genotoxin-induced senescence, the strong and fast activation of the p53/$p21^{CIP1}$ response, as well as the maintenance of this response by unrepaired DNA damage (SCARS) overshadows the impact of $p16^{INK4A}$.

To compare transcriptional alterations in senescent cells induced by B[a]P and IR, RNAseq was performed. Among the top 100 up-regulated genes only 29 were identical between B[a]P and IR expression, among them 6 well-known p53 targets like *TP53INP1* and *CDKN1a*. In contrast, strong similarities were observed comparing the down-regulated genes. Comparing our results to a gene set containing 971 candidate DREAM target genes (DREAM-F) (47) we could show that among 78 genes (out of the top 100 down-regulated genes), which were repressed both, upon B[a]P and IR exposure, 76 were DREAM targets. To verify these results, we additionally utilized a second set (49), containing only 280 potential DREAM targets (DREAM-E). Both DREAM sets overlap in 258 genes. Even using the smaller DREAM target set, among the top 200 down-regulated genes, 119 (B[a]P), 99 (IR) and 76 (Palbociclib) genes were described as DREAM targets (Supplementary Figure S23A). Of note, besides the DREAM pathway, also the RB-E2F pathway might be important for transcriptional repression of p53 targets. In this case, $p21^{CIP1}$ blocks cyclin-CDK complexes, resulting in hypophosphorylation of RB, which induces binding to the activating E2Fs during G0 and G1 and subsequent repression of G1/S genes (67). Indeed, DREAM targets and E2F-RB targets are overlapping, and nearly all repressed E2F-RB targets are also labelled as DREAM-targets (Supplementary Figure S23B). This overlap is stronger using the DREAM-F set than the DREAM-E set. Independent on the set, also DREAM independent E2F-RB targets are repressed upon B[a]P, IR and Palbociclib, indicating that $p21^{CIP1}$ not only represses DREAM targets, but also DREAM-independent E2F-RB targets.

p53-mediated repression occurs mostly *via* activation of $p21^{CIP1}$ and the DREAM complex. However, it was shown that p53 can also repress genes independent on the DREAM complex (33). The authors provide a set of DREAM-dependent p53 targets (DREAM-U) and DREAM-independent p53 targets. The DREAM-U set shows a high similarity with the DREAM-E and DREAM-F sets, whereas the DREAM-independent p53-targets set shows similarity with the DREAM-F, but not the DREAM-E set (Supplementary Figure S24). As expected, B[a]P (145/200), IR (146/200) and Palbo (101/200) treatment showed a high overlap with the DREAM-U set. Opposite, only minor overlap with DREAM-independent p53-targets was observed (B[a]P

(6/200), IR (10/200) and Palbo (4/200)), supporting our finding that the p53 response strongly depends on the DREAM complex upon treatment with B[a]P, IR and Palbociclib.

Among the repressed DREAM targets were the genes coding for the MuvB interactors FOXM1 and B-Myb and the proliferation-associated DREAM/MuvB target genes (*ASPM, AURKB, CENPA, CENPF, PLK1, TK1*). Additionally, DREAM-target genes coding for well-known markers of senescence like *HMGB1*, *HMGB2* and *LMNB1* were also repressed by B[a]P and IR. Overall, the repression of multiple factors involved in cell cycle progression clearly leads to the assumption that inhibition of CDK4 and subsequent activation of the DREAM complex is sufficient to induce and maintain genotoxic stress-induced senescence.

To test this assumption, we applied the CDK4/6 inhibitor Palbociclib. Transcriptomic analysis revealed that Palbociclib also induced a strong repression of the DREAM targets showing a significant overlap with the DREAM targets repressed by B[a]P and IR. Thus, among the top 200 repressed genes, 98 genes were identical, with 95 of them being DREAM targets. These data strongly support our finding that inhibition of CDK4/6 and subsequent activation of the DREAM complex is sufficient for induction of the senescence phenotype. This is further supported by the finding that knockdown of $p21^{CIP1}$, E2F4 and E2F5 diminished the repression of the DREAM targets and subsequently of the senescent phenotype upon B[a]P and IR exposure.

In line with our results, the importance of the DREAM complex in senescence was recently shown (68). In these experiments, human breast fibroblasts, conditionally immortalized using a thermolabile SV40 large T (LT) antigen along with the catalytic subunit of human telomerase (hTERT), underwent senescence upon inactivation of the thermolabile LT antigen. This process was abrogated by simultaneous expression of MMB-FOXM1 complex components (LIN52, B-Myb and FOXM1). Moreover, it was shown that hepatocellular carcinoma evaded RB1-induced replicative senescence by activating the FOXM1–FOXO1 axis (69).

In our previous work, we showed that non-toxic concentrations of B[a]P and BPDE led to p53-dependent transcriptional up-regulation of the nucleotide excision repair (NER) genes *DDB2* and *XPC* and finally to enhanced NER activity and activation of an adaptive response (70). In parallel, a transcriptional repression of the DNA repair genes *MSH2*, *MSH6*, *EXO1* and *RAD51*, and therefore, abrogation of mismatch repair and homologous recombination was observed (58). This repression was also observed upon IR and specifically occurred in senescent cells. These findings are supported by our RNAseq data. Thus, besides cell cycle regulators, also DNA repair factors were significantly repressed by B[a]P and IR. The same was true for Palbociclib. Overall, 11 repair genes were repressed by B[a]P, IR and Palbociclib, 13 by B[a]P and Palbociclib and 6 only by Palbociclib (Supplementary Figure S25). Nearly all these genes also represent DREAM targets. Among these genes were specific factors of the mismatch repair system, homologous recombination and components of the Fanconi complex. For some of these genes (13 out of 30) we already demonstrated their repression using qPCR (58), including the MMR factors *MSH2*, *MSH6*, *EXO1* and the HR factor *RAD51*. However, a repression of *MSH6* (in NGS data set) was observed only upon Palbociclib exposure, the repression upon B[a]P and IR was not strong enough ($\log_2 = -1$). This weak repression reflects our previous results (58) and suggests that the abrogation of MSH6 protein expression is most likely caused by the repression of its stabilizing binding partner MSH2. Concerning BER and NER, only factors which were also involved in replication (FEN1, PCNA, POLE and LIG1), but none of the key-factors were repressed. The DREAM-dependent regulation of the DNA repair is in line with recent data from the Schumacher group. In their recent work, they showed the DREAM complex also represents a master regulator of somatic DNA repair capacities in *Caenorhabditis elegans* and in mice, highlighting the importance of this mechanism among different species (71).

Our data suggest that the DREAM complex plays an important role in turning the cell cycle arrest irreversible, both in G2/M-arrested cells and in cells that slip through the M-phase with DNA damage (see Figure 7F). Whereas Palbociclib-mediated inhibition of CDK4/6 occurs immediately, resulting in a strong activation of the DREAM complex and inhibition of the E2F1/FOXM1/MYBL2 pathways in G1, it is not clear at which stage CDK4 gets inhibited upon DNA damage. It is thought that the formation of DSBs during the S-phase represents the main DDR trigger, which leads to an immediate intra S-phase arrest. However, this intra-S arrest seems not to be strong enough and the cells finish DNA synthesis and progress into the G2-phase with damaged DNA. At this stage the DDR is activated and $p21^{CIP1}$, as well as CHK1/2 inhibit CDK1 and CDK2, which triggers a G2/M arrest. However, in the case of B[a]P and IR, most cells (67% upon B[a]P and 78% upon IR) can escape the G2/M-arrest and progress through mitosis into a second G1-phase. At this time point, $p21^{CIP1}$ is fully activated and inhibits CDK4, activating the DREAM complex. This leads to transcriptional repression of multiple factors described above, irreversibly arresting the cell in the second G1-phase and also in the first G2/M phase. As consequence, only a small fraction of the cells can progress into the second S, G2 and M-phase or even undergo mitotic bypass. We should note that besides CDK4 also CDK6 might play an important role in genotoxin-induced DREAM activation and senescence, however we were not able to detect interaction between $p21^{CIP1}$ and CDK6. Obviously, the role of CDK6 in DNA-damage induced senescence has to be addressed in further studies.

Overall, $p21^{CIP1}$ plays two different roles during DNA damage-induced senescence. First, it induces a G2/M arrest *via* inhibition of CDK1/2. However, this arrest is only transient, and in a second step, the $p21^{CIP1}$/CDK4/DREAM axis irreversibly arrests the cells in the first G2/M or the subsequent G1/S or G2/M-phase.

Data availability

Interactomics data are deposited at the Protein Identification Database (PRIDE). Project Name: Protein-protein interactions of p21CIP1 in MCF7 cells during cellular senescence, Project accession: PXD042908 Raw transcriptomics data are available at GEO (Gene expression omnibus) under GSE234862 (Impact of benzoapyrene and ionizing radiation on gene expression of MCF7 cells) and GSE235350 (Impact of Palbociclib (PD-0332991; CDK4/6 inhibitor) on gene expression of MCF7 cells).

Supplementary data

Supplementary Data are available at NAR Online.

Acknowledgements

This work was funded by the Deutsche Forschungsgemeinschaft (German Research Foundation) – Project-ID 393547839 – SFB 1361 - TP05 to MC, Project-ID 393547839 – SFB 1361 - TP19 to TH, Project-ID 393547839 – SFB 1361 - TP14 to AL, as well as by the Deutsche Forschungsgemeinschaft (German Research Foundation) project CH 665/8–1 to MC. We acknowledge that this work was funded by the Deutsche Forschungsgemeinschaft (DFG, German Research Foundation) – Project-ID 393547839 – SFB 1361, through the support of the IMB Genomics Core Facility and the use of its NextSeq500.

Funding

Deutsche Forschungsgemeinschaft [393547839 – SFB 1361, CH 665/8-1]. Funding for open access charge: Deutsche Forschungsgemeinschaft (German Research Foundation) [393547839 – SFB 1361].

Conflict of interest statement

None declared.

References

1. Hayflick,L. (1965) The limited in vitro lifetime of Human diploid cell strains. *Exp. Cell. Res.*, **37**, 614–636.
2. d'Adda di Fagagna,F. (2008) Living on a break: cellular senescence as a DNA-damage response. *Nat. Rev. Cancer*, **8**, 512–522.
3. Muller,M. (2009) Cellular senescence: molecular mechanisms, in vivo significance, and redox considerations. *Antioxid. Redox Signal.*, **11**, 59–98.
4. Fridman,A.L. and Tainsky,M.A. (2008) Critical pathways in cellular senescence and immortalization revealed by gene expression profiling. *Oncogene*, **27**, 5975–5987.
5. Cichowski,K. and Hahn,W.C. (2008) Unexpected pieces to the senescence puzzle. *Cell*, **133**, 958–961.
6. Stein,G.H., Drullinger,L.F., Soulard,A. and Dulic,V. (1999) Differential roles for cyclin-dependent kinase inhibitors p21 and p16 in the mechanisms of senescence and differentiation in human fibroblasts. *Mol. Cell. Biol.*, **19**, 2109–2117.
7. Fiorentino,F.P., Symonds,C.E., Macaluso,M. and Giordano,A. (2009) Senescence and p130/Rbl2: a new beginning to the end. *Cell Res.*, **19**, 1044–1051.
8. Alcorta,D.A., Xiong,Y., Phelps,D., Hannon,G., Beach,D. and Barrett,J.C. (1996) Involvement of the cyclin-dependent kinase inhibitor p16 (INK4a) in replicative senescence of normal human fibroblasts. *Proc. Nat. Acad. Sci. U.S.A.*, **93**, 13742–13747.
9. Ohtani,N., Imamura,Y., Yamakoshi,K., Hirota,F., Nakayama,R., Kubo,Y., Ishimaru,N., Takahashi,A., Hirao,A., Shimizu,T., *et al.* (2007) Visualizing the dynamics of p21(Waf1/Cip1) cyclin-dependent kinase inhibitor expression in living animals. *Proc. Nat. Acad. Sci. U.S.A.*, **104**, 15034–15039.
10. Robles,S.J. and Adami,G.R. (1998) Agents that cause DNA double strand breaks lead to p16INK4a enrichment and the premature senescence of normal fibroblasts. *Oncogene*, **16**, 1113–1123.
11. Beausejour,C.M., Krtolica,A., Galimi,F., Narita,M., Lowe,S.W., Yaswen,P. and Campisi,J. (2003) Reversal of human cellular senescence: roles of the p53 and p16 pathways. *EMBO J.*, **22**, 4212–4222.
12. Takahashi,A., Ohtani,N., Yamakoshi,K., Iida,S., Tahara,H., Nakayama,K., Nakayama,K.I., Ide,T., Saya,H. and Hara,E. (2006) Mitogenic signalling and the p16INK4a-Rb pathway cooperate to enforce irreversible cellular senescence. *Nat. Cell Biol.*, **8**, 1291–1297.
13. Hara,E., Smith,R., Parry,D., Tahara,H., Stone,S. and Peters,G. (1996) Regulation of p16CDKN2 expression and its implications for cell immortalization and senescence. *Mol. Cell. Biol.*, **16**, 859–867.
14. Khan,S., Guevara,C., Fujii,G. and Parry,D. (2004) p14ARF is a component of the p53 response following ionizing irradiation of normal human fibroblasts. *Oncogene*, **23**, 6040–6046.
15. Weinberg,R.A. (1995) The retinoblastoma protein and cell cycle control. *Cell*, **81**, 323–330.
16. Dimova,D.K. and Dyson,N.J. (2005) The E2F transcriptional network: old acquaintances with new faces. *Oncogene*, **24**, 2810–2826.
17. AACR Project GENIE Consortium (2017) AACR Project GENIE: powering precision medicine through an international consortium. *Cancer Discov.*, **7**, 818–831.
18. Litovchick,L., Sadasivam,S., Florens,L., Zhu,X., Swanson,S.K., Velmurugan,S., Chen,R., Washburn,M.P., Liu,X.S. and DeCaprio,J.A. (2007) Evolutionarily conserved multisubunit RBL2/p130 and E2F4 protein complex represses human cell cycle-dependent genes in quiescence. *Mol. Cell*, **26**, 539–551.
19. Schmit,F., Korenjak,M., Mannefeld,M., Schmitt,K., Franke,C., von Eyss,B., Gagrica,S., Hanel,F., Brehm,A. and Gaubatz,S. (2007) LINC, a human complex that is related to pRB-containing complexes in invertebrates regulates the expression of G2/M genes. *Cell Cycle*, **6**, 1903–1913.
20. Chen,X., Muller,G.A., Quaas,M., Fischer,M., Han,N., Stutchbury,B., Sharrocks,A.D. and Engeland,K. (2013) The forkhead transcription factor FOXM1 controls cell cycle-dependent gene expression through an atypical chromatin binding mechanism. *Mol. Cell. Biol.*, **33**, 227–236.
21. Guiley,K.Z., Iness,A.N., Saini,S., Tripathi,S., Lipsick,J.S., Litovchick,L. and Rubin,S.M. (2018) Structural mechanism of Myb-MuvB assembly. *Proc. Nat. Acad. Sci. U.S.A.*, **115**, 10016–10021.
22. Pilkinton,M., Sandoval,R. and Colamonici,O.R. (2007) Mammalian Mip/LIN-9 interacts with either the p107, p130/E2F4 repressor complex or B-myb in a cell cycle-phase-dependent context distinct from the Drosophila dREAM complex. *Oncogene*, **26**, 7535–7543.
23. Sadasivam,S., Duan,S. and DeCaprio,J.A. (2012) The MuvB complex sequentially recruits B-Myb and FoxM1 to promote mitotic gene expression. *Genes Dev.*, **26**, 474–489.
24. Litovchick,L., Florens,L.A., Swanson,S.K., Washburn,M.P. and DeCaprio,J.A. (2011) DYRK1A protein kinase promotes quiescence and senescence through DREAM complex assembly. *Genes Dev.*, **25**, 801–813.
25. Marceau,A.H., Felthousen,J.G., Goetsch,P.D., Iness,A.N., Lee,H.W., Tripathi,S.M., Strome,S., Litovchick,L. and Rubin,S.M. (2016) Structural basis for LIN54 recognition of CHR elements in cell cycle-regulated promoters. *Nat. Commun.*, **7**, 12301.
26. Farkas,T., Hansen,K., Holm,K., Lukas,J. and Bartek,J. (2002) Distinct phosphorylation events regulate p130- and p107-mediated repression of E2F-4. *J. Biol. Chem.*, **277**, 26741–26752.
27. Cobrinik,D. (2005) Pocket proteins and cell cycle control. *Oncogene*, **24**, 2796–2809.
28. Hansen,K., Farkas,T., Lukas,J., Holm,K., Ronnstrand,L. and Bartek,J. (2001) Phosphorylation-dependent and -independent functions of p130 cooperate to evoke a sustained G1 block. *EMBO J.*, **20**, 422–432.
29. Grant,G.D., Brooks,L. 3rd, Zhang,X., Mahoney,J.M., Martyanov,V., Wood,T.A., Sherlock,G., Cheng,C. and Whitfield,M.L. (2013) Identification of cell cycle-regulated genes periodically expressed in U2OS cells and their regulation by FOXM1 and E2F transcription factors. *Mol. Biol. Cell*, **24**, 3634–3650.
30. Quaas,M., Muller,G.A. and Engeland,K. (2012) p53 can repress transcription of cell cycle genes through a p21(WAF1/CIP1)-dependent switch from MMB to DREAM

protein complex binding at CHR promoter elements. *Cell Cycle*, **11**, 4661–4672.
31. Fischer,M., Quaas,M., Steiner,L. and Engeland,K. (2016) The p53-p21-DREAM-CDE/CHR pathway regulates G2/M cell cycle genes. *Nucleic Acids Res.*, **44**, 164–174.
32. Fischer,M., Quaas,M., Nickel,A. and Engeland,K. (2015) Indirect p53-dependent transcriptional repression of Survivin, CDC25C, and PLK1 genes requires the cyclin-dependent kinase inhibitor p21/CDKN1A and CDE/CHR promoter sites binding the DREAM complex. *Oncotarget*, **6**, 41402–41417.
33. Uxa,S., Bernhart,S.H., Mages,C.F.S., Fischer,M., Kohler,R., Hoffmann,S., Stadler,P.F., Engeland,K. and Muller,G.A. (2019) DREAM and RB cooperate to induce gene repression and cell-cycle arrest in response to p53 activation. *Nucleic Acids Res.*, **47**, 9087–9103.
34. Baan,R., Grosse,Y., Straif,K., Secretan,B., El Ghissassi,F., Bouvard,V., Benbrahim-Tallaa,L., Guha,N., Freeman,C., Galichet,L., *et al.* (2009) A review of human carcinogens–part F: chemical agents and related occupations. *Lancet Oncol.*, **10**, 1143–1144.
35. Borgen,A., Darvey,H., Castagnoli,N., Crocker,T.T., Rasmussen,R.E. and Wang,I.Y. (1973) Metabolic conversion of benzo(a)pyrene by Syrian hamster liver microsomes and binding of metabolites to deoxyribonucleic acid. *J. Med. Chem.*, **16**, 502–506.
36. Huberman,E., Sachs,L., Yang,S.K. and Gelboin,V. (1976) Identification of mutagenic metabolites of benzo(a)pyrene in mammalian cells. *Proc. Nat. Acad. Sci. U.S.A.*, **73**, 607–611.
37. Newbold,R.F. and Brookes,P. (1976) Exceptional mutagenicity of a benzo(a)pyrene diol epoxide in cultured mammalian cells. *Nature*, **261**, 52–54.
38. Slaga,T.J., Viaje,A., Betty,D.L., Brachen,W., Buty,S.G. and Scribner,J.D. (1976) Skin tumor initiating ability of benzo(a)pyrene 4,5- 7,5- and 7,8-diol-9,10-epoxides and 7,8-diol. *Cancer Lett.*, **2**, 115–121.
39. Hockley,S.L., Arlt,V.M., Brewer,D., Giddings,I. and Phillips,D.H. (2006) Time- and concentration-dependent changes in gene expression induced by benzo(a)pyrene in two human cell lines, MCF-7 and HepG2. *Bmc Genomics [Electronic Resource]*, **7**, 260.
40. Osborne,M.R., Beland,F.A., Harvey,R.G. and Brookes,P. (1976) The reaction of (+/-)-7alpha, 8beta-dihydroxy-9beta, 10beta-epoxy-7,8,9,10-tetrahydrobenzo(a)pyrene with DNA. *Int. J. Cancer*, **18**, 362–368.
41. Christmann,M., Tomicic,M.T., Roos,W.P. and Kaina,B. (2003) Mechanisms of human DNA repair: an update. *Toxicology*, **193**, 3–34.
42. Duijndam,B., Goudriaan,A., van den Hoorn,T., van der Stel,W., Le Devedec,S., Bouwman,P., van der Laan,J.W. and van de Water,B. (2021) Physiologically relevant estrogen receptor alpha pathway reporters for single-cell imaging-based carcinogenic hazard assessment of estrogenic compounds. *Toxicol. Sci.*, **181**, 187–198.
43. Platt,K. and Oesch,F. (1983) Efficient synthesis of non-K-region trans-dihydro diols of polycyclic aromatic hydrocarbons from o-quinones and catechols. *J. Org. Chem.*, **48**, 265–268.
44. Yagi,H., Thakker,D.R., Hernandez,O., Koreeda,M. and Jerina,D.M. (1977) Synthesis and reactions of the highly mutagenic 7,8-diol 9,10-epoxides of the carcinogen benzo[a]pyrene. *J. Am. Chem. Soc.*, **99**, 1604–1611.
45. Aasland,D., Gotzinger,L., Hauck,L., Berte,N., Meyer,J., Effenberger,M., Schneider,S., Reuber,E.E., Roos,W.P., Tomicic,M.T., *et al.* (2019) Temozolomide induces senescence and repression of DNA repair pathways in glioblastoma cells via activation of ATR-CHK1, p21, and NF-kappaB. *Cancer Res.*, **79**, 99–113.
46. Subramanian,A., Tamayo,P., Mootha,V.K., Mukherjee,S., Ebert,B.L., Gillette,M.A., Paulovich,A., Pomeroy,S.L., Golub,T.R., Lander,E.S., *et al.* (2005) Gene set enrichment analysis: a knowledge-based approach for interpreting genome-wide expression profiles. *Proc. Nat. Acad. Sci. U.S.A.*, **102**, 15545–15550.
47. Fischer,M., Grossmann,P., Padi,M. and DeCaprio,J.A. (2016) Integration of TP53, DREAM, MMB-FOXM1 and RB-E2F target gene analyses identifies cell cycle gene regulatory networks. *Nucleic Acids Res.*, **44**, 6070–6086.
48. Shepard,J.L., Amatruda,J.F., Stern,H.M., Subramanian,A., Finkelstein,D., Ziai,J., Finley,K.R., Pfaff,K.L., Hersey,C., Zhou,Y., *et al.* (2005) A zebrafish bmyb mutation causes genome instability and increased cancer susceptibility. *Proc. Nat. Acad. Sci. U.S.A.*, **102**, 13194–13199.
49. Engeland,K. (2018) Cell cycle arrest through indirect transcriptional repression by p53: i have a DREAM. *Cell Death Differ.*, **25**, 114–132.
50. Christmann,M. and Kaina,B. (2000) Nuclear translocation of mismatch repair proteins MSH2 and MSH6 as a response of cells to alkylating agents. *J. Biol. Chem.*, **275**, 36256–36262.
51. Reich,T.R., Schwarzenbach,C., Vilar,J.B., Unger,S., Muhlhausler,F., Nikolova,T., Poplawski,A., Baymaz,H.I., Beli,P., Christmann,M., *et al.* (2021) Localization matters: nuclear-trapped Survivin sensitizes glioblastoma cells to temozolomide by elevating cellular senescence and impairing homologous recombination. *Cell. Mol. Life Sci.*, **78**, 5587–5604.
52. Finzel,A., Grybowski,A., Strasen,J., Cristiano,E. and Loewer,A. (2016) Hyperactivation of ATM upon DNA-PKcs inhibition modulates p53 dynamics and cell fate in response to DNA damage. *Mol. Biol. Cell*, **27**, 2360–2367.
53. Rodier,F., Munoz,D.P., Teachenor,R., Chu,V., Le,O., Bhaumik,D., Coppe,J.P., Campeau,E., Beausejour,C.M., Kim,S.H., *et al.* (2011) DNA-SCARS: distinct nuclear structures that sustain damage-induced senescence growth arrest and inflammatory cytokine secretion. *J. Cell Sci.*, **124**, 68–81.
54. Todd,M.C., Langan,T.A. and Sclafani,R.A. (2017) Doxycycline-regulated p16(MTS1) expression suppresses the Anchorage-independence and tumorigenicity of breast cancer cell lines that lack endogenous p16. *J. Cancer*, **8**, 190–198.
55. Sun,A., Bagella,L., Tutton,S., Romano,G. and Giordano,A. (2007) From G0 to S phase: a view of the roles played by the retinoblastoma (Rb) family members in the Rb-E2F pathway. *J. Cell. Biochem.*, **102**, 1400–1404.
56. Ferreira,R., Magnaghi-Jaulin,L., Robin,P., Harel-Bellan,A. and Trouche,D. (1998) The three members of the pocket proteins family share the ability to repress E2F activity through recruitment of a histone deacetylase. *Proc. Nat. Acad. Sci. U.S.A.*, **95**, 10493–10498.
57. Meloni,A.R., Smith,E.J. and Nevins,J.R. (1999) A mechanism for Rb/p130-mediated transcription repression involving recruitment of the CtBP corepressor. *Proc. Nat. Acad. Sci. U.S.A.*, **96**, 9574–9579.
58. Allmann,S., Mayer,L., Olma,J., Kaina,B., Hofmann,T.G., Tomicic,M.T. and Christmann,M. (2020) Benzo[a]pyrene represses DNA repair through altered E2F1/E2F4 function marking an early event in DNA damage-induced cellular senescence. *Nucleic Acids Res.*, **48**, 12085–12101.
59. Atadja,P., Wong,H., Veillette,C. and Riabowol,K. (1995) Overexpression of cyclin D1 blocks proliferation of normal diploid fibroblasts. *Exp. Cell. Res.*, **217**, 205–216.
60. Schade,A.E., Fischer,M. and DeCaprio,J.A. (2019) RB, p130 and p107 differentially repress G1/S and G2/M genes after p53 activation. *Nucleic Acids Res.*, **47**, 11197–11208.
61. Wagner,V. and Gil,J. (2020) Senescence as a therapeutically relevant response to CDK4/6 inhibitors. *Oncogene*, **39**, 5165–5176.
62. Maskey,R.S., Wang,F., Lehman,E., Wang,Y., Emmanuel,N., Zhong,W., Jin,G., Abraham,R.T., Arndt,K.T., Myers,J.S., *et al.* (2021) Sustained mTORC1 activity during palbociclib-induced growth arrest triggers senescence in ER+ breast cancer cells. *Cell Cycle*, **20**, 65–80.
63. Sakaue-Sawano,A., Kurokawa,H., Morimura,T., Hanyu,A., Hama,H., Osawa,H., Kashiwagi,S., Fukami,K., Miyata,T.,

Miyoshi,H., *et al.* (2008) Visualizing spatiotemporal dynamics of multicellular cell-cycle progression. *Cell*, **132**, 487–498.
64. Di Leonardo,A., Linke,S.P., Clarkin,K. and Wahl,G.M. (1994) DNA damage triggers a prolonged p53-dependent G1 arrest and long-term induction of Cip1 in normal human fibroblasts. *Genes Dev.*, **8**, 2540–2551.
65. Herbig,U., Jobling,W.A., Chen,B.P., Chen,D.J. and Sedivy,J.M. (2004) Telomere shortening triggers senescence of human cells through a pathway involving ATM, p53, and p21(CIP1), but not p16(INK4a). *Mol. Cell*, **14**, 501–513.
66. Rayess,H., Wang,M.B. and Srivatsan,E.S. (2012) Cellular senescence and tumor suppressor gene p16. *Int. J. Cancer*, **130**, 1715–1725.
67. Dyson,N.J. (2016) RB1: a prototype tumor suppressor and an enigma. *Genes Dev.*, **30**, 1492–1502.
68. Kumari,R., Hummerich,H., Shen,X., Fischer,M., Litovchick,L., Mittnacht,S., DeCaprio,J.A. and Jat,P.S. (2021) Simultaneous expression of MMB-FOXM1 complex components enables efficient bypass of senescence. *Sci. Rep.*, **11**, 21506.
69. Chand,V., Liao,X., Guzman,G., Benevolenskaya,E. and Raychaudhuri,P. (2022) Hepatocellular carcinoma evades RB1-induced senescence by activating the FOXM1-FOXO1 axis. *Oncogene*, **41**, 3778–3790.
70. Christmann,M., Boisseau,C., Kitzinger,R., Berac,C., Allmann,S., Sommer,T., Aasland,D., Kaina,B. and Tomicic,M.T. (2016) Adaptive upregulation of DNA repair genes following benzo(a)pyrene diol epoxide protects against cell death at the expense of mutations. *Nucleic Acids Res.*, **44**, 10727–10743.
71. Bujarrabal-Dueso,A., Sendtner,G., Meyer,D.H., Chatzinikolaou,G., Stratigi,K., Garinis,G.A. and Schumacher,B. (2023) The DREAM complex functions as conserved master regulator of somatic DNA-repair capacities. *Nat. Struct. Mol. Biol.*, **30**, 475–488.

Received: November 9, 2023. **Revised:** May 2, 2024. **Editorial Decision:** May 3, 2024. **Accepted:** May 14, 2024